Supporting Information

Impact of Incoherent Coupling within Localized Surface Plasmon Resonance on Singlet Oxygen Production in Rose Bengal-Modified Silica-Coated Silver Nanoshells (SiO_2@Ag@SiO_2-RB).

Vladimir Kabanov and Belinda Heyne*

Department of Chemistry, University of Calgary,
2500 University Drive NW, Calgary, Alberta, Canada, T2N 1N4

*Email: bjmheyne@ucalgary.ca

Table of Contents:

1. Transmission Electron Microscopy 2
2. Nanoparticle Concentration Estimations 14
3. ζ Potential Measurements 15
4. Raman Spectroscopy 15
5. UV-Visible-NIR Spectra 16
6. Extinction, Absorption and Scattering Deconvolution 17
7. Silver Nanoshell Etching 19
8. Direct Detection of Singlet Oxygen Emission 19
9. Steady-State Fluorescence Emission 25
10. Indirect Detection of Singlet Oxygen 28
11. Integrated Absorption Analysis 32
References 35

1. Transmission Electron Microscopy

Nanoparticle sizes were characterized using transmission electron micrographs obtained on a TEM Hitachi H-7650 (Microscopy and Imaging Facility, University of Calgary). Samples were prepared on carbon-coated Cu TEM grids. Values for the diameter of the nanoparticles are based on at least 150 measurements.

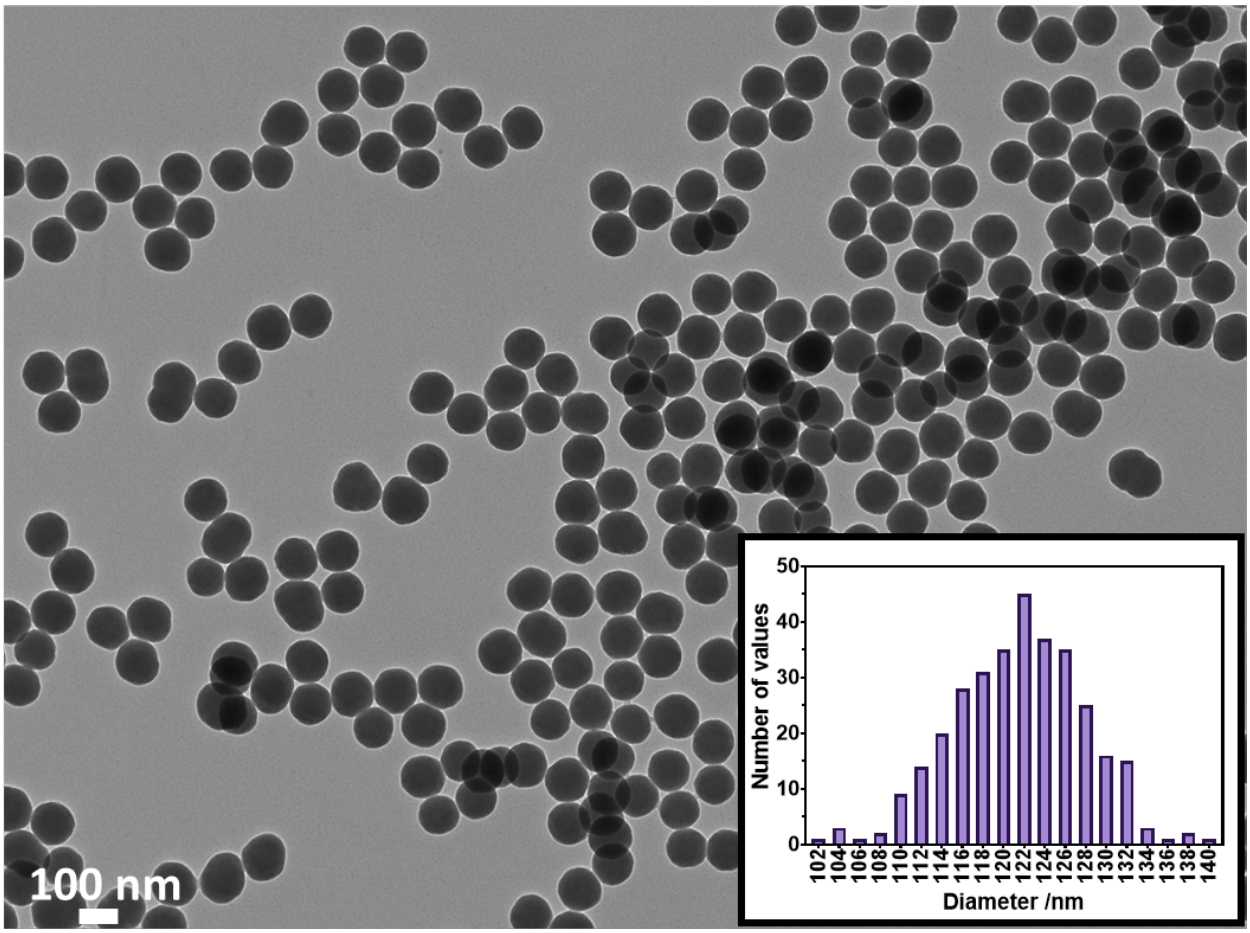

Figure S1: TEM image of silica nanoparticles with mean diameter and standard deviation of 121 ± 6 nm, obtained from the size distribution shown in the inset.

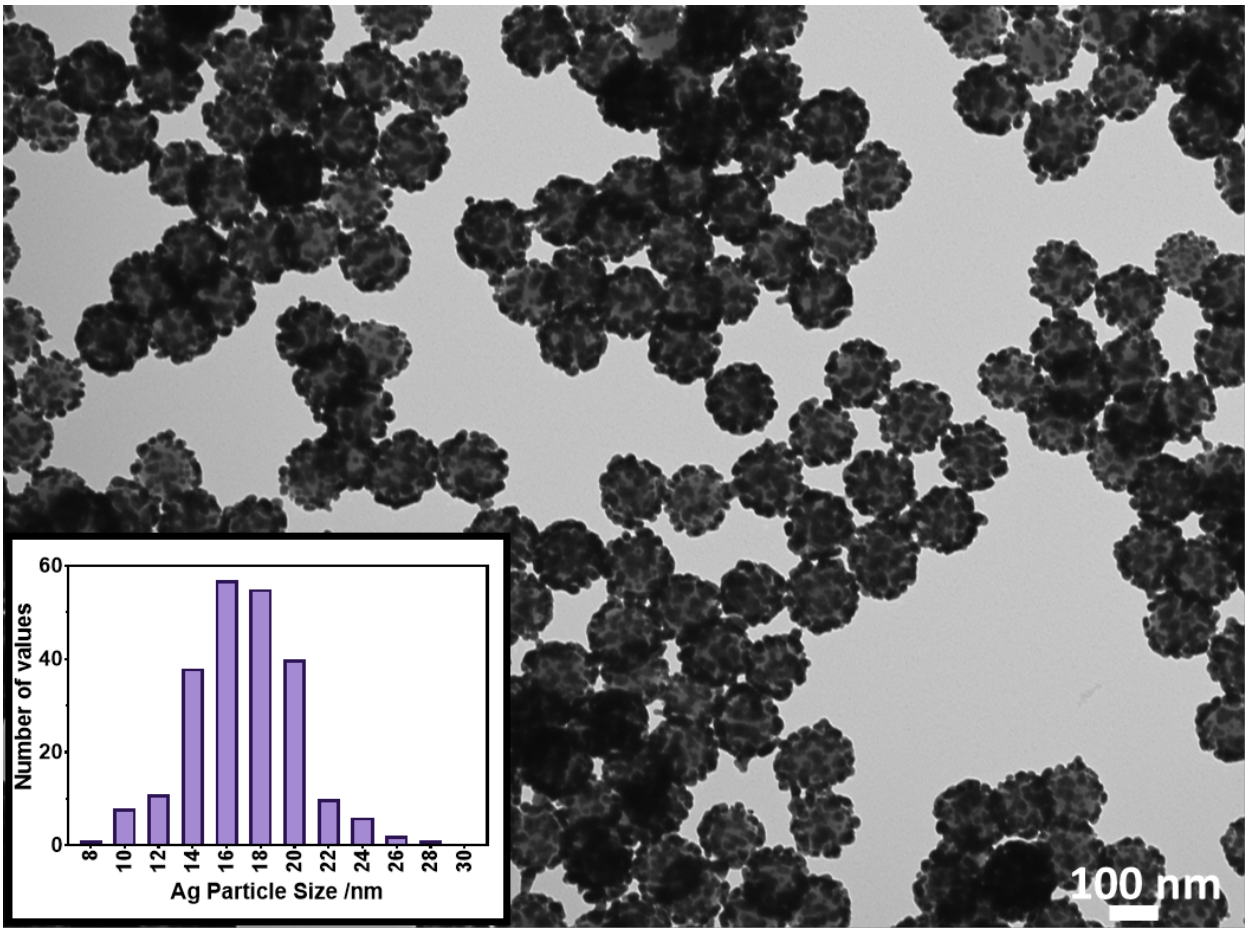

Figure S2: TEM image of silica nanoparticles coated in incomplete silver shells (SiO_2@$Ag_{(i)}$); mean diameter and standard deviation of silver particle of the surface was determined to be 17 ± 3 nm, obtained from the size distribution shown in the inset.

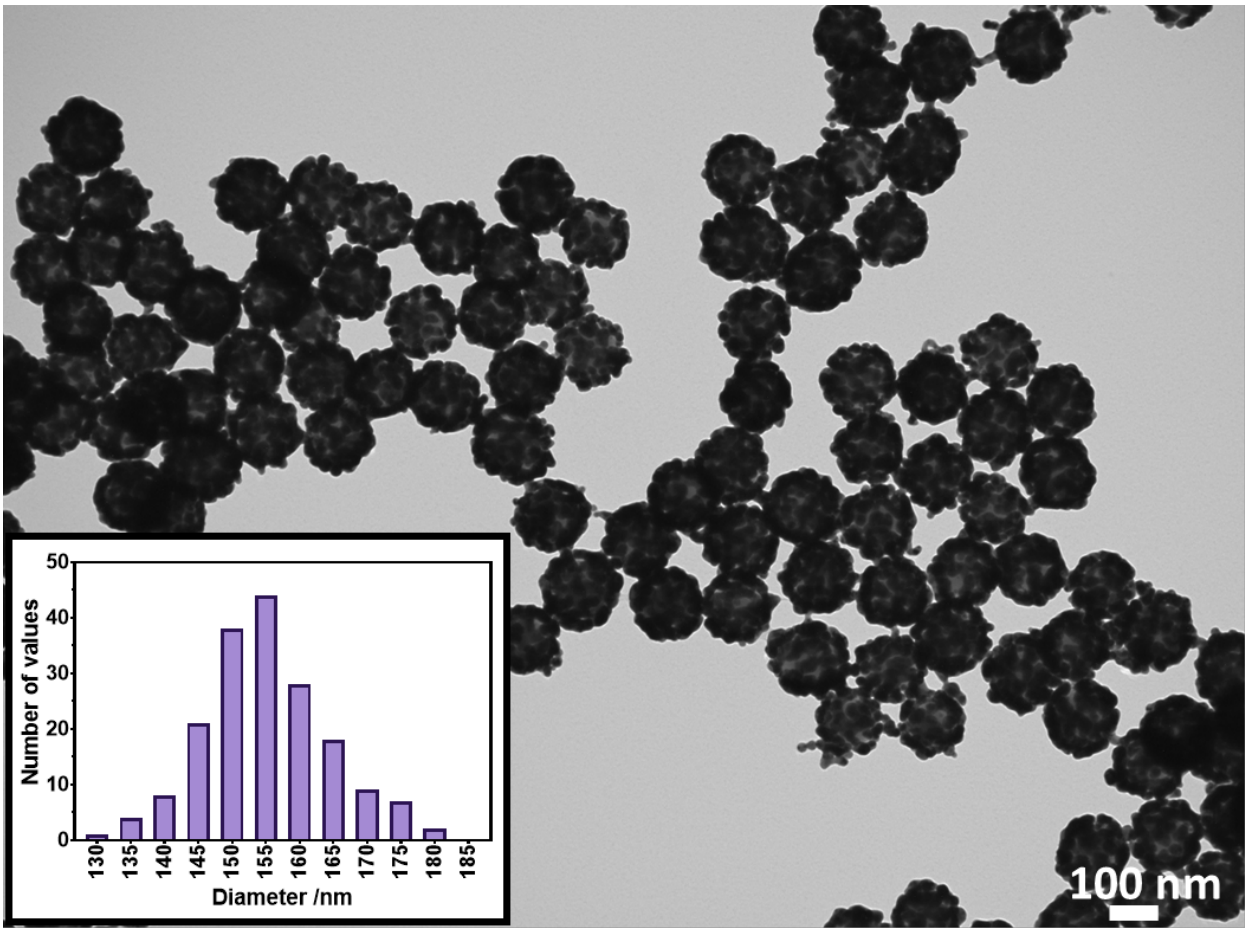

Figure S3: TEM image of silica nanoparticles with partial silver shells (SiO_2@$Ag_{(p)}$) with overall particles' mean diameter and standard deviation of 155 ± 9 nm, obtained from the size distribution shown in the inset.

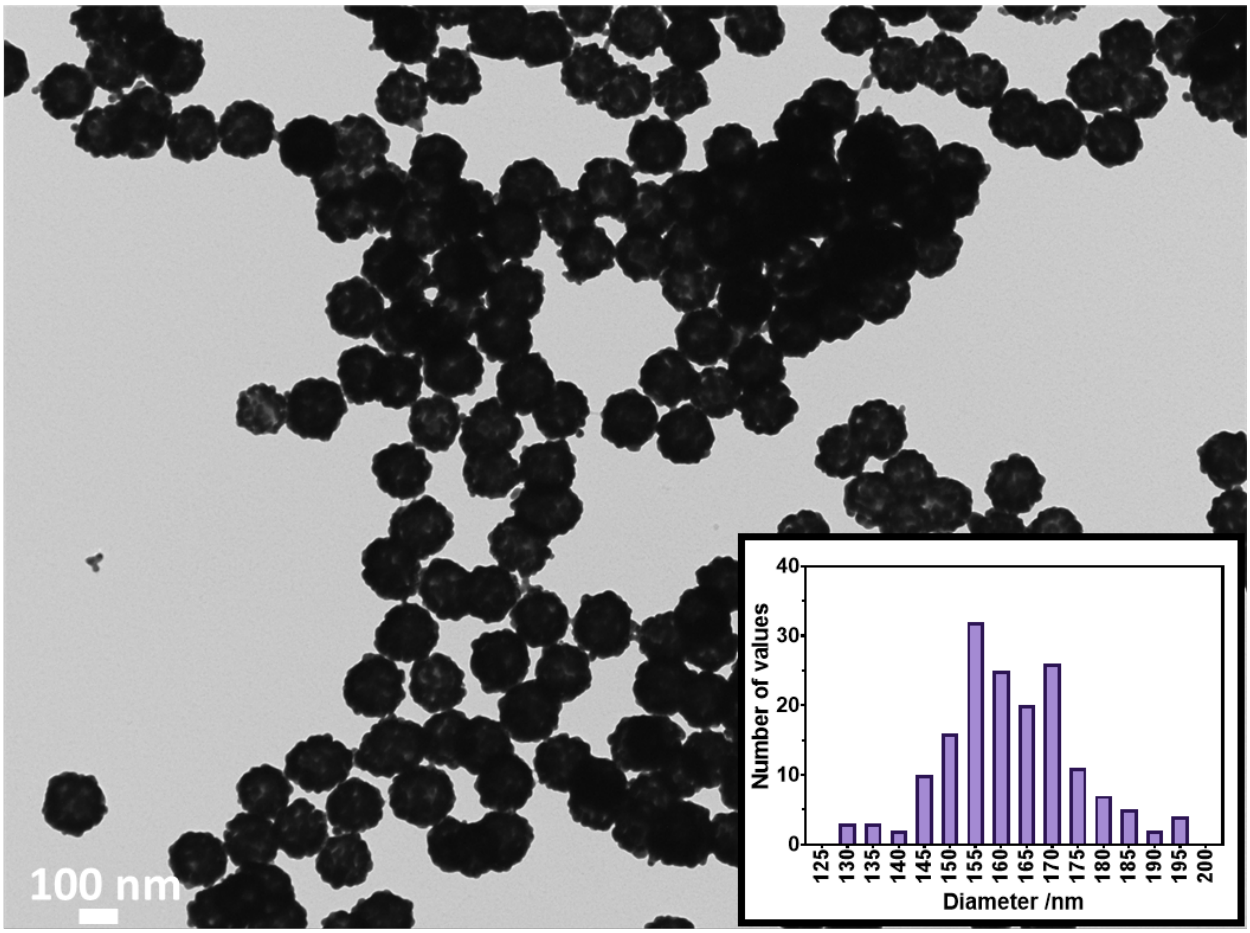

Figure S4: TEM image of silica nanoparticles with complete silver shells (SiO_2@$Ag_{(c)}$) with overall particles' mean diameter and standard deviation of 163 ± 13 nm, obtained from the size distribution shown in the inset.

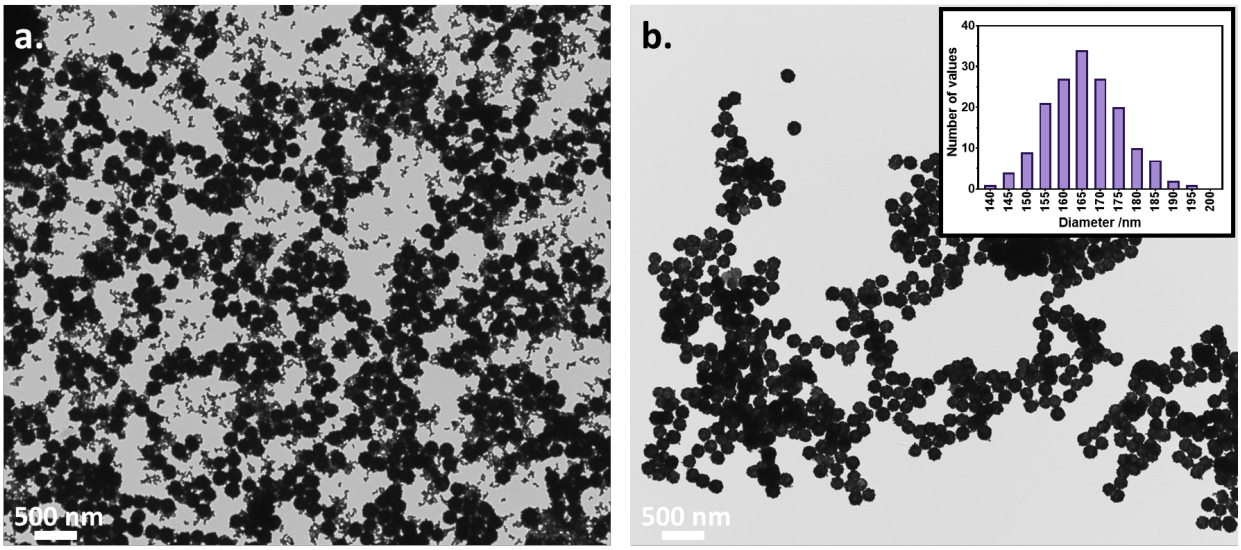

Figure S5: TEM images of (a) as prepared, and (b) purified SiO_2@$Ag_{(c)}$ nanoparticles prepared using 0.01 mg/mL SiO_2 in the silver deposition protocol; overall purified particles' mean diameter and standard deviation was found to be 166 ± 10 nm obtained from the size distribution shown in the inset.

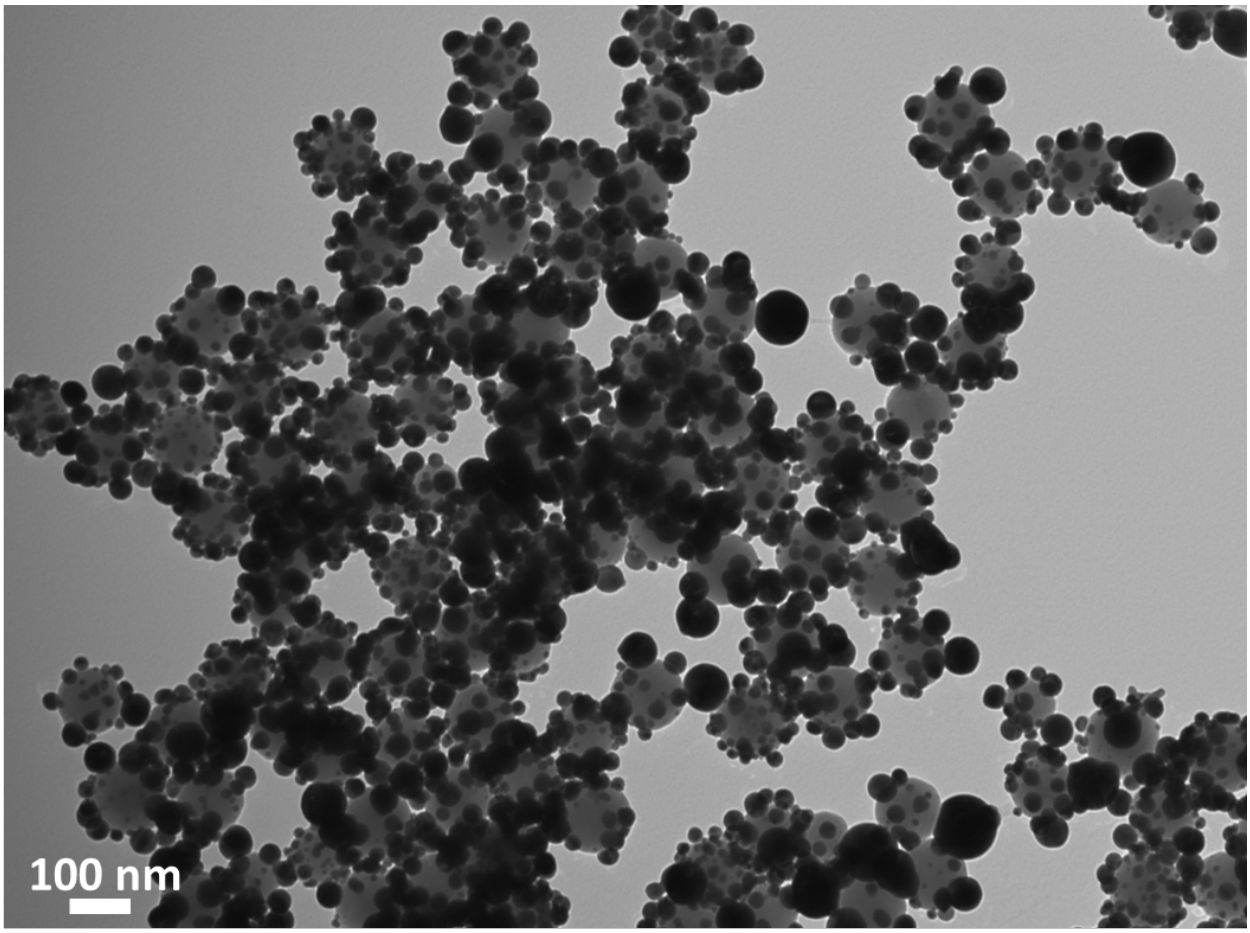

Figure S6: TEM image of SiO_2@$Ag_{(c)}$ nanoparticles after being subjected to 3mJ pulsed 532 nm laser irradiation for 30 seconds in an attempt to melt and reforge a shell without defect.

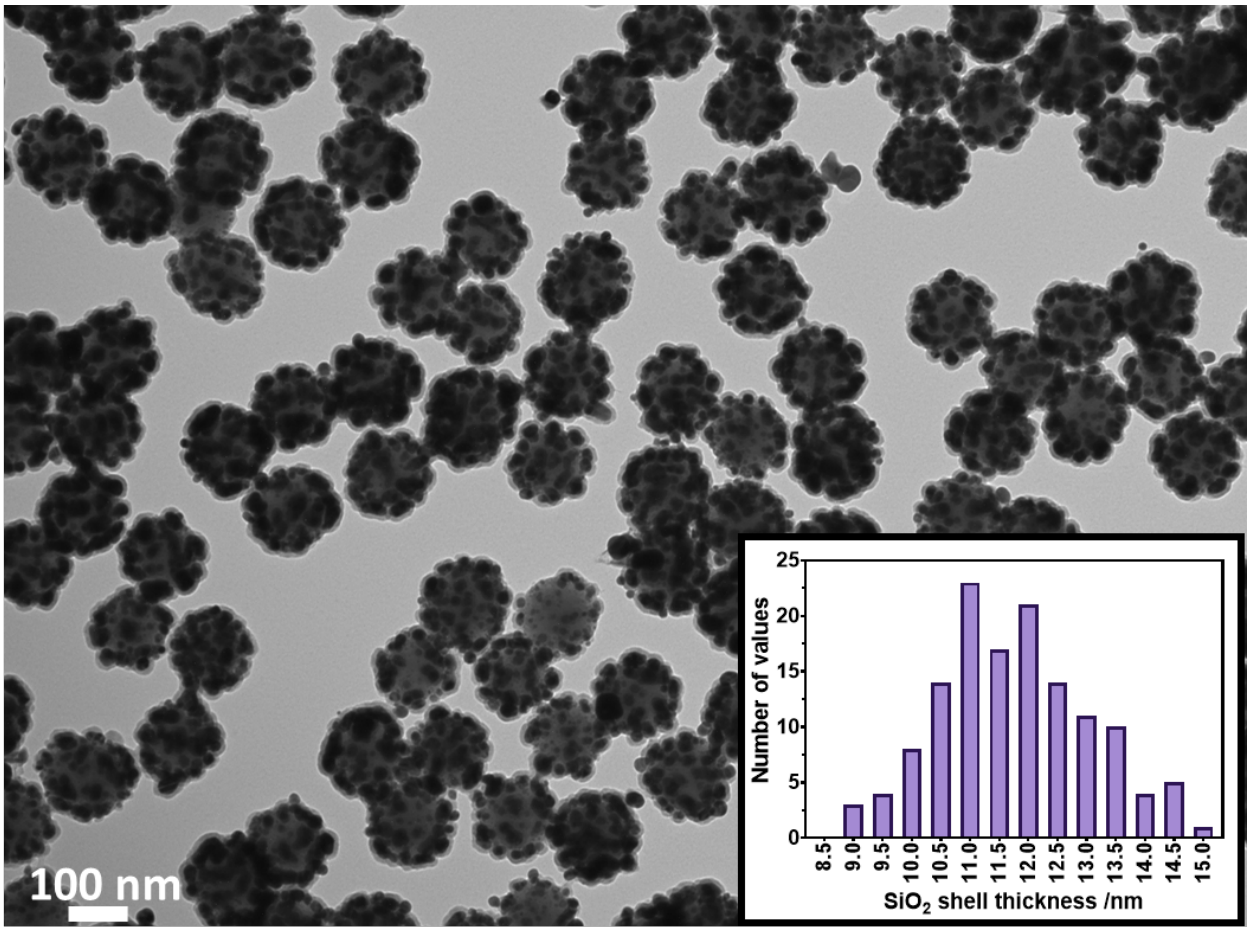

Figure S7: TEM image of SiO_2@$Ag_{(i)}$@SiO_2 nanoparticles with outer silica shell mean thickness and standard deviation of 12 ± 1 nm, obtained from the size distribution shown in the inset.

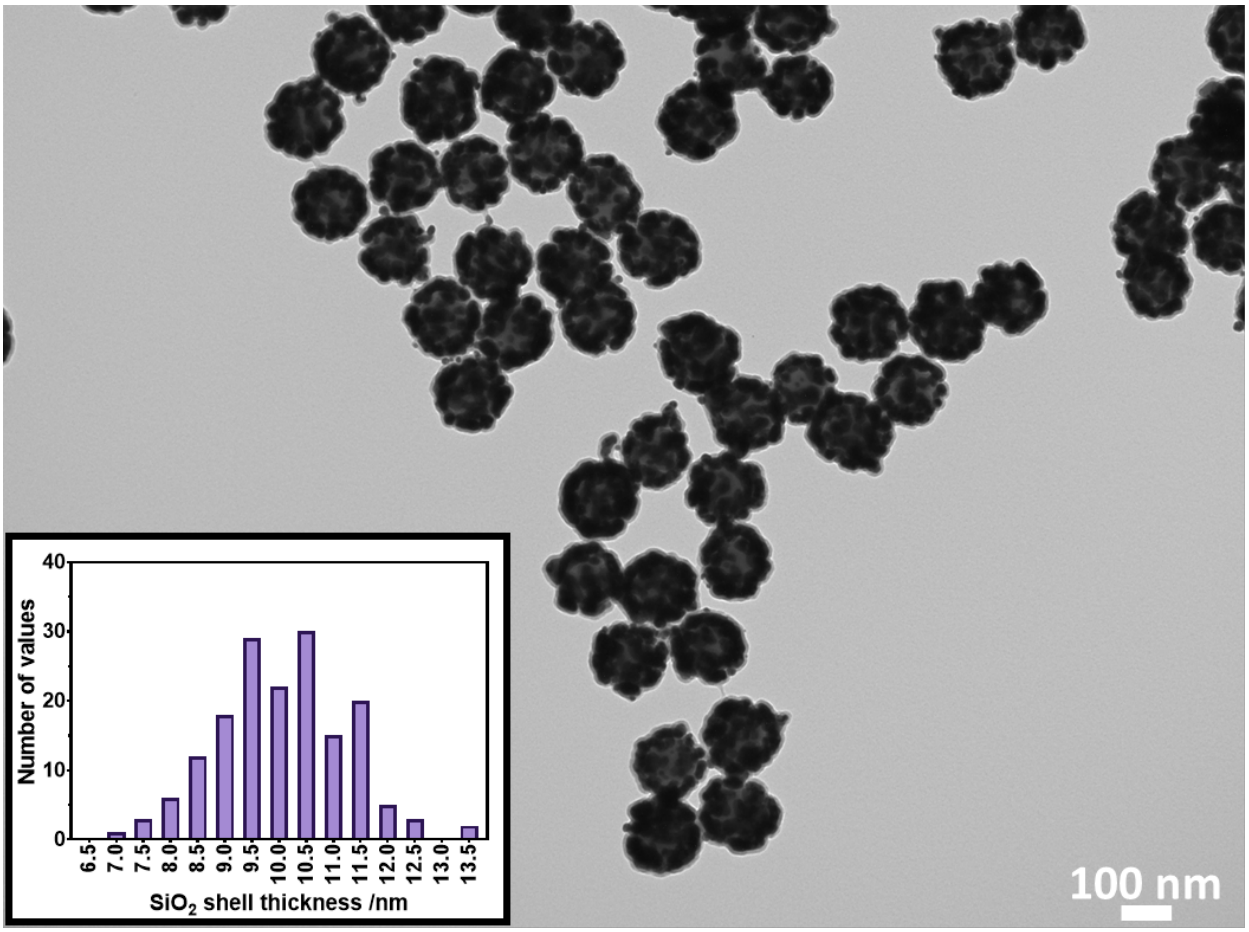

Figure S8: TEM image of SiO_2@$Ag_{(p)}$@SiO_2 nanoparticles with outer silica shell mean thickness and standard deviation of 10 ± 1 nm, obtained from the size distribution shown in the inset.

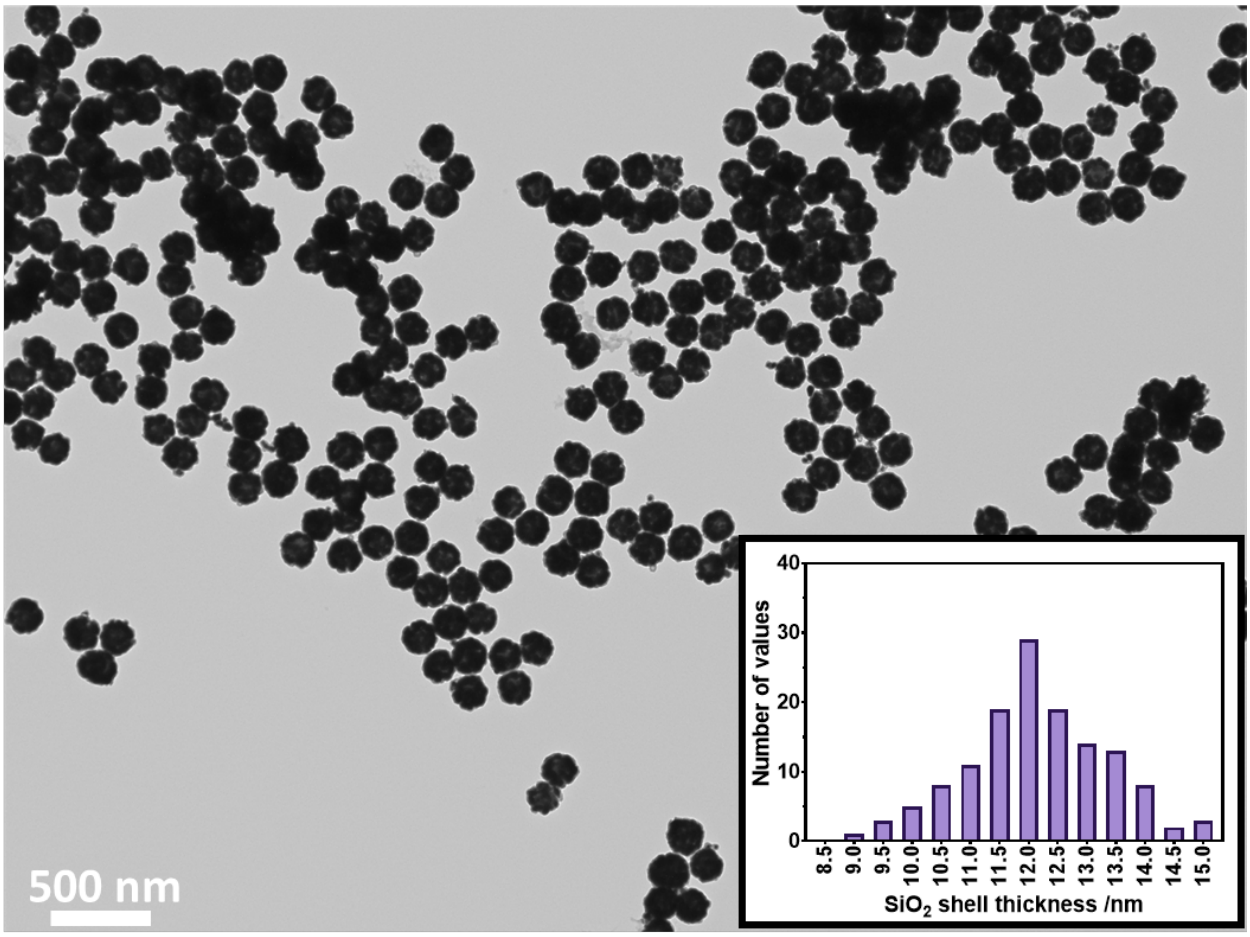

Figure S9: TEM image of SiO_2@$Ag_{(c)}$@SiO_2 nanoparticles with outer silica shell mean thickness and standard deviation of 12 ± 1 nm, obtained from the size distribution shown in the inset.

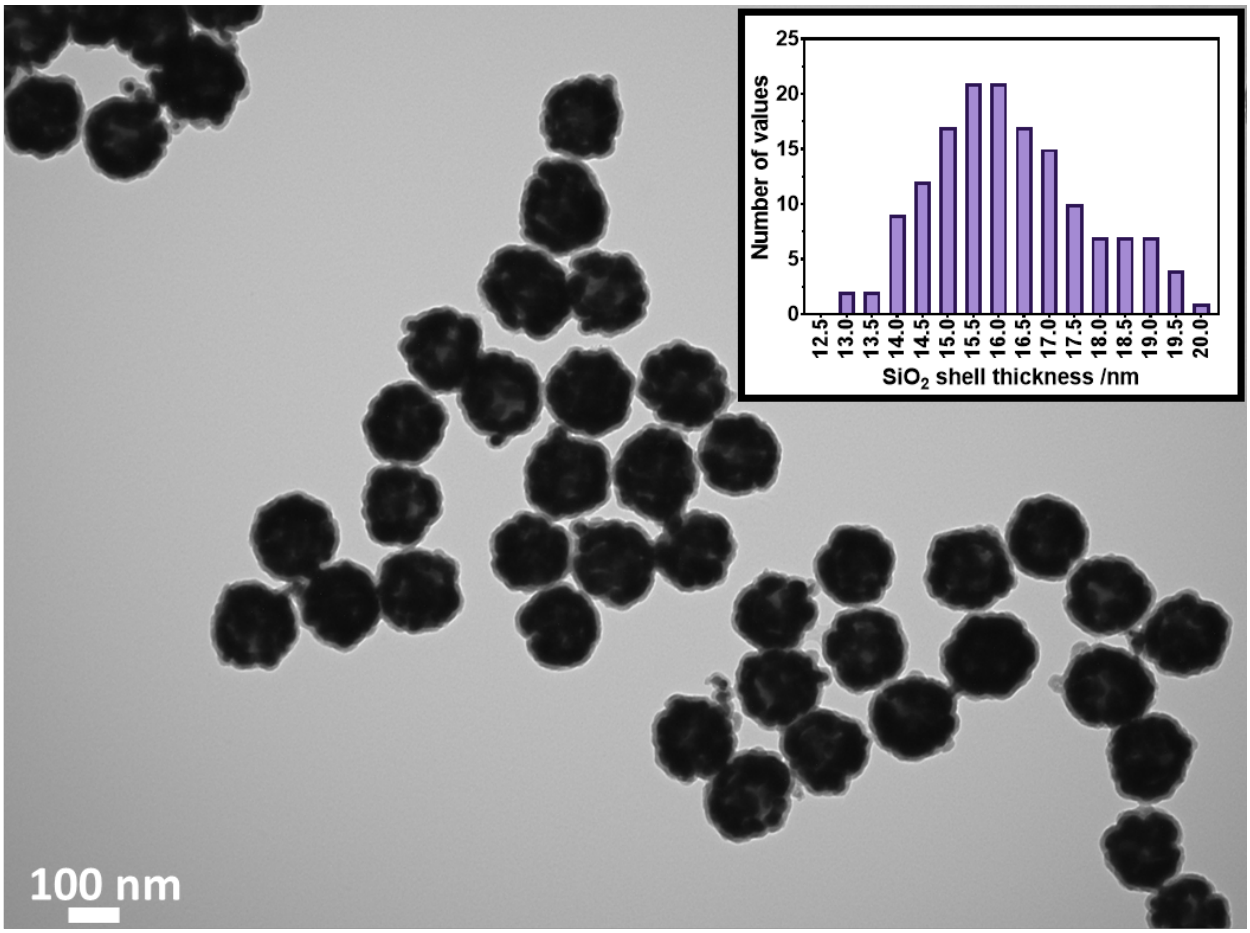

Figure S10: TEM image of SiO_2@$Ag_{(c)}$@SiO_2 nanoparticles with thicker outer silica shell of 16 ± 2 nm, obtained from the size distribution shown in the inset.

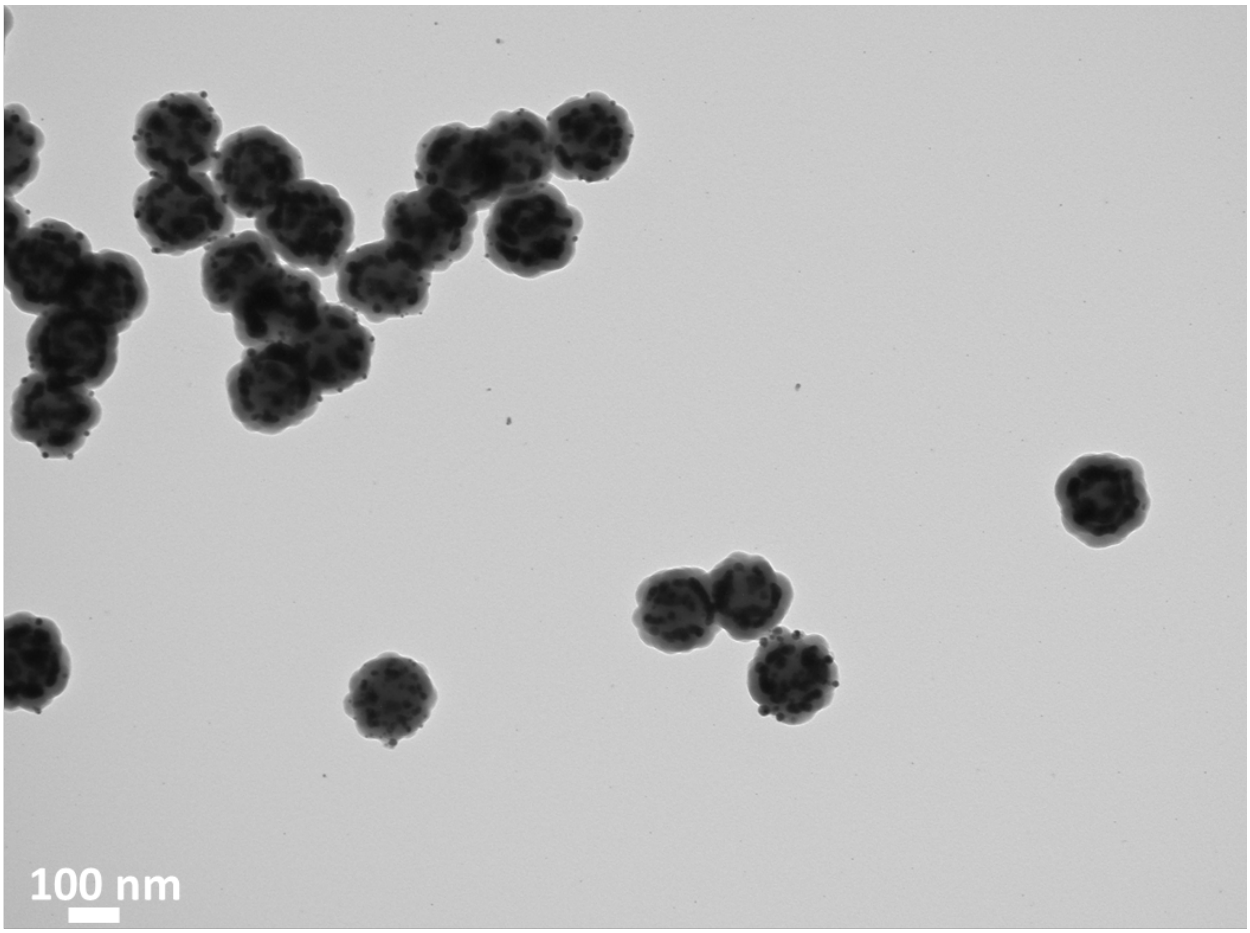

Figure S11: TEM image of SiO_2@$Ag_{(c)}$@SiO_2 nanoparticles after attempted synthesis of >20nm thick outer silica shells.

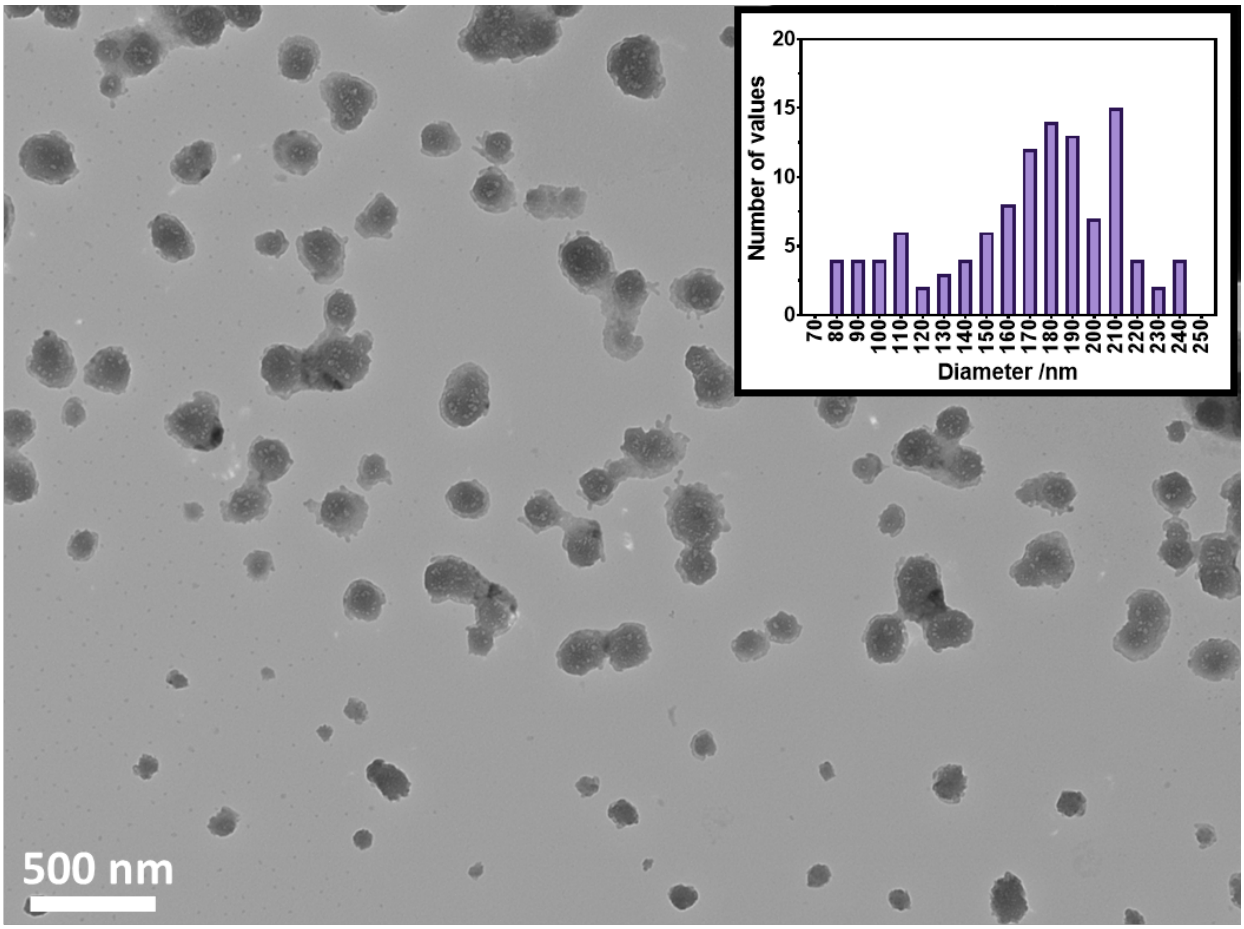

Figure S12: TEM image of SiO_2@$Ag_{(c)}$@SiO_2 nanoparticles after 12-hour incubation in the 0.25M $NaCl_{(aq)}$ solution, centrifugation and redispersion into pure H_2O; inset shows the size distribution of particles found in the sample.

2. Nanoparticle Concentration Estimations

Concentrations of the of SiO_2@Ag@SiO_2 nanoparticles used throughout the experiments can be estimated by first considering the mean SiO_2-core nanoparticle volume derived from TEM images (Figure S1), and the density of amorphous silica (2.2g/cm^3).[1]

$$V_{SiO_2\ particle} = \frac{4}{3}\pi r^3 = \frac{4}{3}\pi\,(60.5 \times 10^{-7}\ cm)^3 = 9.28\ \times\ 10^{-16}\ cm^3$$

$$m_{SiO_2\ particle} = \left(2.2\ \frac{g}{cm^3}\right) \times\ (9.28 \times\ 10^{-16}\ cm^3) = 2.04\ \times\ 10^{-15}\ g$$

By drying and weighing an aliquot of SiO_2-core nanoparticle solution post-synthesis and purification, it was determined that 1 batch of SiO_2-core particles, synthesized following the protocol described in main text, produces 315 mg of SiO_2. With this knowledge the SiO_2-core particles stock solution was prepared at 10 mg/mL concentration and from this solution 250 µL (2.5 mg of SiO_2 cores) was used for SiO_2@$Ag_{(c)}$ synthesis, 500 µL (5 mg of SiO_2 cores) was used for SiO_2@$Ag_{(p)}$ synthesis, and 1000 µL (10 mg of SiO_2 cores) was used for SiO_2@$Ag_{(i)}$ synthesis. Meaning the molar amounts of particles in each shell deposition reaction was, as follows:

For complete shells:

$$N_{SiO_2} = \frac{2.5 \times\ 10^{-3}\ g}{2.04\ \times\ 10^{-15}\ g/particle} = 1.23 \times\ 10^{12}\ particles$$

$$n_{SiO_2} = 1.23 \times\ 10^{12}\ particles\ /\ \left(6.022\ \times\ 10^{23}\ \frac{particle}{mol}\right) = 2.04 \times\ 10^{-12}\ mol$$

For partial shells:

$$n_{SiO_2} = 4.09\ \times\ 10^{-12}\ mol$$

For incomplete shells:

$$n_{SiO_2} = 8.17\ \times\ 10^{-12}\ mol$$

Since no free SiO_2-core particle were ever observed in the TEM we can assume 100% for shell deposition efficiency. Furthermore, assuming no nanoparticles were lost as a result of centrifugation, the above calculated molar amounts of SiO_2-core particles equate directly to the per-batch molar amounts of silver coated particles, and ultimately the SiO_2@Ag@SiO_2 and SiO_2@Ag@SiO_2-RB nanoparticles.

3. ζ Potential Measurements

Surface charge of the nanoparticles was measured in ethanol for all samples, except for SiO_2@$Ag_{(c)}$@SiO_2-RB which was measured in H_2O, using Zetasizer Nano (Malvern) instrument (λ_{ex} = 640 nm). In all cases nanoparticle concentration was kept low as to not exceed optical density of 0.05 at 640 nm.

4. Raman Spectroscopy

Raman spectra were obtained on Bruker's Vertex 70 high resolution FTIR spectrometer equipped with a RAM II FT-Raman module. Samples were excited by Nd:YAG laser at 1064 nm. For each sample, triplicate measurements were performed with signal integration set to 5 minutes per measurement. The resulting Raman spectra were averaged between the triplicates to reduce noise.

Dry Rose Bengal di-sodium salt powder (95% dye content) was analyzed as obtained from Sigma Aldrich without further purification.

2 full batches of purified SiO_2@$Ag_{(c)}$@SiO_2-RB nanoparticles (~2 pmol/batch, as synthesized according to the details in main text) were centrifuged at 4500×g for 30 minutes, the supernatant was discarded, and the nanoparticle pellets were allowed to air-dry for >48 hours. Dry SiO_2@$Ag_{(c)}$@SiO_2-RB nanoparticles powder was combined, loaded into a capillary tube and analyzed.

As a control experiment, 2 full batches of SiO_2@$Ag_{(c)}$@SiO_2 nanoparticles were prepared and dispersed in 10 mL of H_2O at pH adjusted to ~4 using dilute HCl. To this suspension RB was added to a final concentration of 0.1 mM. The solution was left to stir overnight, then washed via centrifugation at 4500×g for 30 minutes several times until the supernatant appeared mostly colourless. The SiO_2@$Ag_{(c)}$@SiO_2 nanoparticles with adsorbed RB were then allowed to air-dry for >48 hours, after which the dry powder sample was loaded into a capillary tube and analyzed.

5. UV-Visible-NIR Spectra

Broadband extinction spectra were obtained using Varian Cary 5000 UV-Visible-NIR spectrophotometer with diffraction grating transition set to 900 nm and the lamp change set to 800 nm.

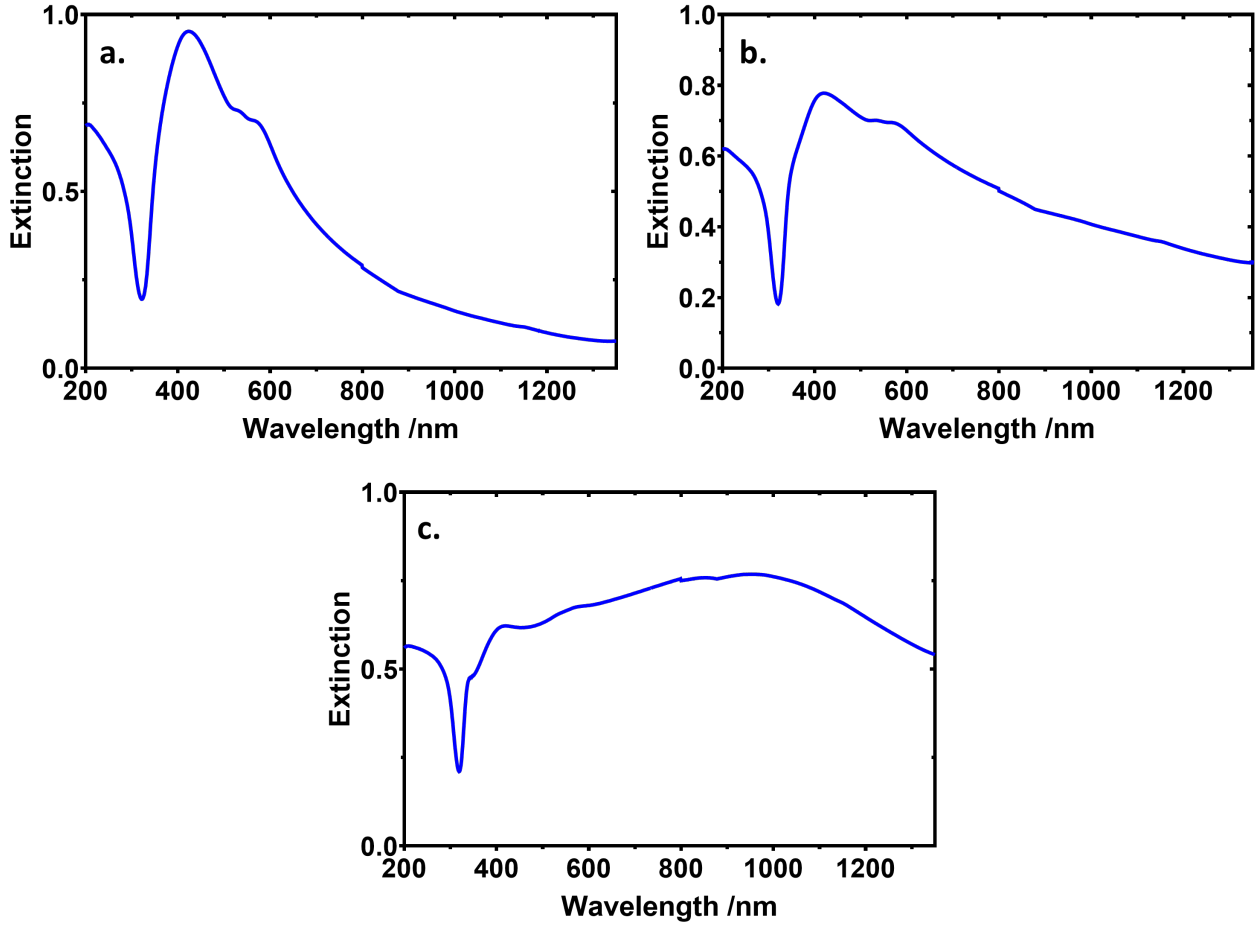

Figure S13: Broadband extinction spectra of ~10 pM dispersions of (a) SiO_2@$Ag_{(i)}$@SiO_2-RB, (b) SiO_2@$Ag_{(p)}$@SiO_2-RB, and (c) SiO_2@$Ag_{(c)}$@SiO_2-RB nanoparticles in H_2O.

6. Extinction, Absorption and Scattering Deconvolution

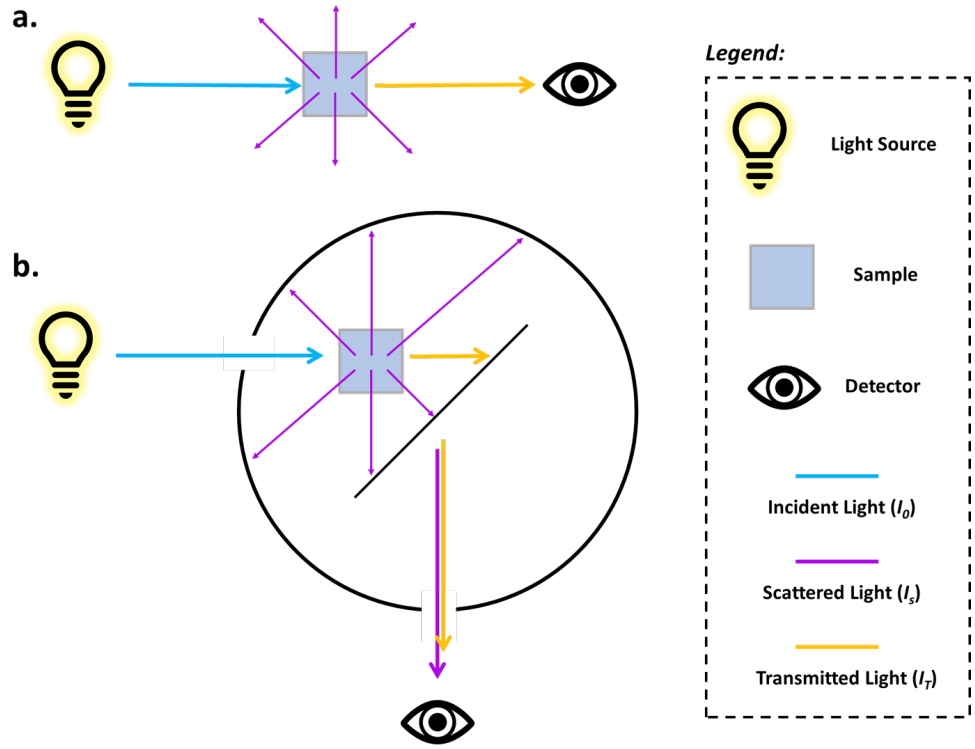

Figure S14: Schematic illustration of the methods used to acquire extinction and absorption spectra for the nanoparticle samples. UV-Vis spectrophotometer set-up (a) is used to acquire extinction spectra; emission spectrophotometer equipped with an integrating sphere set-up (b) is used to acquire light source spectra through the blank sample and through the NPs' suspension sample which are then used to extract nanoparticles absorption spectra. Figure adapted with modifications from reference 2.

Deconvolution of the nanoparticles extinction spectra into their absorption and scattering components was performed following our previously reported protocols.[2, 3] When considering irradiation of a sample with incident light of intensity I_0, several things can occur, namely: light can be transmitted by the sample (I_T), it can be scattered (I_s), absorbed (I_A), or reflected by the cuvette walls (I_R). The overall relationship between the different light intensities is given by equation S1.

$$I_0 = I_A + I_T + I_s + I_R \qquad (S1)$$

Assuming that the forward scattering is negligible when compared to the total scattering by the NP suspension, and that the intensity of light reflected by the cuvette walls is much smaller than the total intensity of light incident on the sample ($I_R <<< I_0$) a UV-Vis absorption and an integrating sphere equipped emission spectrophotometer can be used to obtain extinction and absorption spectrum, respectively. In the case of performing a measurement on a NP suspension using a UV-Vis spectrophotometer, light which reaches the detector is dominated by the I_T (figure S14a), in other words the transmission of the sample is approximated by equation S2, and the obtained spectrum is a combination of light lost largely due to

sample's absorption and scattering. An extinction spectrum can therefore be obtained by performing a UV-Vis measurement across a range of wavelengths.

$$T_{UV-Vis} = \frac{I_T}{I_0} \qquad (S2)$$

On the other hand, measuring the same sample inside of the integrating sphere set up in the emission spectrophotometer (figure S14b) results in the detection of both the scattered light and the transmitted light (equation S3). In other words, the light intensity lost in this measurement is largely due to the absorption by the sample, meaning an absorption spectrum can be obtained by performing this measurement for a nanoparticle suspension sample.

$$T_{Integrating\ Sphere} = \frac{I_T + I_s}{I_0} \qquad (S3)$$

The difference between the extinction and the absorption spectra obtained experimentally on the nanoparticle samples can then also be calculated at each wavelength and used to construct a scattering spectrum.

A Varian Cary 50 UV-Vis spectrophotometer was used for extinction measurements. The baseline was obtained on a blank sample of solvent (H_2O), and the measurement was performed in "absorption" scan mode. An Edinburgh FLS900 spectrometer equipped with a xenon lamp as a light source and an Integrating Sphere Assembly (F-M01) was used for absorption measurements. First the excitation and emission wavelengths were both set to at λ = 468 nm (peak of the xenon lamp emission) and the slits were adjusted to optimize signal intensity counts (maximized just below the saturation count of ~$2x10^6$). The instrument was then set up to perform a synchronous scan in the range of 800 nm – 300 nm. A blank sample scan was performed on a cuvette containing H_2O, followed by a scan of the nanoparticles' aqueous suspension. From the two scans, absorption spectra were extracted using a software package provided by Edinburgh Instruments.

7. Silver Nanoshell Etching

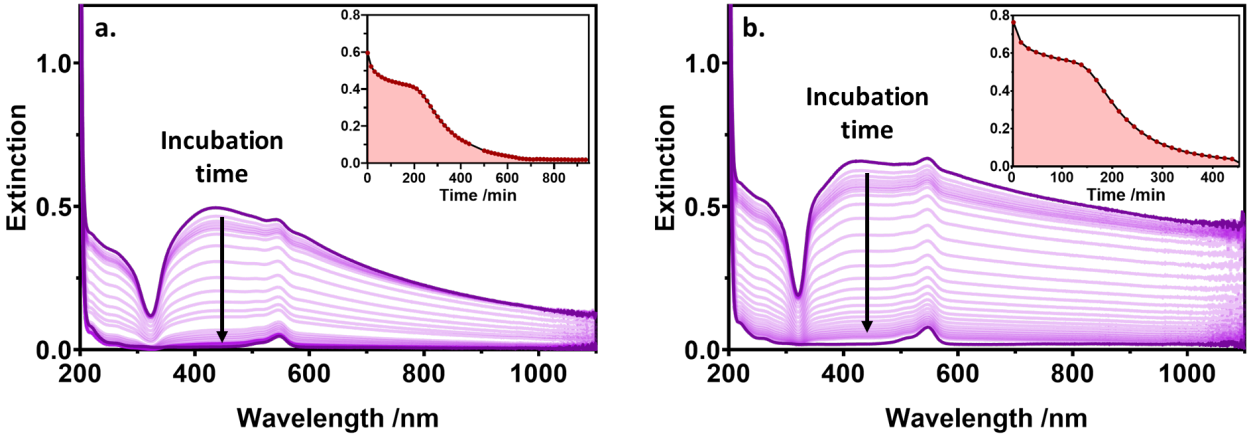

Figure S15: Changes to the extinction of a 10pM dispersion of (a) SiO_2@$Ag_{(i)}$@SiO_2-RB; and (b) SiO_2@$Ag_{(p)}$@SiO_2-RB nanoparticles in 0.25M $NaCl_{(aq)}$, insets show the respective evolution of peak extinction over the time of the experiment.

8. Direct Detection of Singlet Oxygen Emission

Time resolved near-infrared (NIR) phosphorescence of $^1O_2$ was detected using a customized system.[4, 5] A diode-pumped pulsed Nd:YAG laser (FTSS355-Q3, CryLaS GmbH, Berlin, Germany) working at 1 kHz repetition rate at 532 nm was used for excitation. A 1064 nm rugate notch filter (Edmund Optics, York, U.K.) and a 1150 nm long-pass filter (FEL1150, ThorLabs, Newton, NJ) were placed at the exit port of the laser to remove any residual component of its fundamental emission in the near-infrared region. The $^1O_2$ luminescence from the sample was detected at 90° angle via a Hamamatsu NIR detector (H10330A-45, TE-cooled and operating at -908 V) coupled to a grating monochromator (Spectral Products, Digikröm CM110-1/8 m). Photon counting was achieved with a multichannel scaling card (TimeHarp 260-NANO, PicoQuant GmbH, Germany).

The rate of $^1O_2$ production is equal to the rate of ^{3}PS decay (k_T), with the time constant of the process is being the triplet lifetime τ_T $(= 1/k_T)$. Once produced, $^1O_2$ will disappear with a lifetime, τ_Δ, mostly through non-radiative processes ($k_{\Delta, nr}$),[6] but with a minor fraction of $^1O_2$ molecules (~1 in 10^5) loosing energy by emitting in the near-infrared spectral region ($k_{\Delta, r}$).[7] Therefore, the basic kinetic parameters that contribute to the $^1O_2$ production and decay are the ^{3}PS lifetime, τ_T, and the $^1O_2$ lifetime, τ_Δ $(=1/(k_{\Delta, nr} + k_{\Delta, r}))$. Consequently, the phosphorescence signal (S_t) of $^1O_2$ detected at 1270 nm presents a rise and decay bi-exponential behaviour, which can be modelled by the expression given by equation S4 for heterogeneous systems, i.e. photosensitizer conjugated to SiO_2, with subscripts *1* and *2* indicating the two separate local $^1O_2$ deactivation environments, i.e. bulk-solvent vs. SiO_2 matrix.[8, 9] S_0 is the measure of the signal strength, directly linked to the amount of singlet oxygen in each environment, while the term Y_0 is added to account for the baseline in the real measurement.[10]

$$S_t = S_{0,1} \times \frac{\tau_{\Delta_1}}{\tau_{\Delta_1} - \tau_T} \times e^{-\frac{t}{\tau_{\Delta_1}}} + S_{0,2} \times \frac{\tau_{\Delta_2}}{\tau_{\Delta_2} - \tau_T} \times e^{-\frac{t}{\tau_{\Delta_2}}} - \left(S_{0,1} \times \frac{\tau_{\Delta_1}}{\tau_{\Delta_1} - \tau_T} + S_{0,2} \times \frac{\tau_{\Delta_2}}{\tau_{\Delta_2} - \tau_T} \right) \times e^{-\frac{t}{\tau_T}} \qquad (S4)$$

For the purposes of this study, the signal strength (S_0) of the total $^1O_2$ emission is particularly of interest to assess the overall ability of the nanoparticles to produce the cytotoxic agent. Thus, equation S4, can be simplified to equation S5 suitable to analyse $^1O_2$ emission from the nanoparticles by treating the system as a homogeneous environment.[5, 11, 12]

$$S_t = S_0 \times \frac{\tau_\Delta}{\tau_\Delta - \tau_T} \times \left(e^{-t/\tau_\Delta} - e^{-t/\tau_T}\right) + Y_0 \qquad (S5)$$

Singlet oxygen phosphorescence decay signals were collected at 1270 nm. All samples were irradiated at 532 nm excitation wavelength, and the decay curves for the samples in H_2O were collected for 600 seconds, while for samples in 99% D_2O for 300 seconds. The signals were collected with 256 ns resolution. The kinetic traces were least-squares fitted with equation S5 typically in 1024 ns to 300000 ns time window using Prism 8.0 software (GraphPad Software Inc., La Jolla, CA) with τ_Δ, τ_T, S_0 and Y_0 as free parameters. The quality of the fittings was assessed by the residual plots. The experimental results and fit parameters are summarized in figures S16 – S20, and table S1.

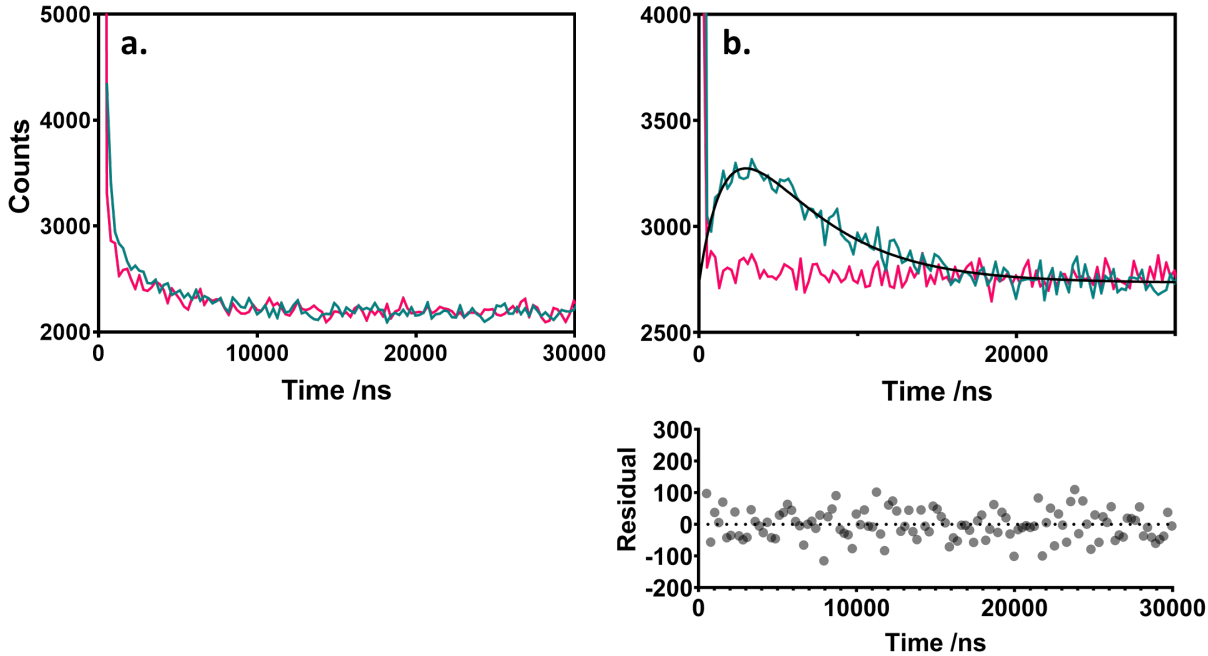

Figure S16: Time resolved direct detection of $^1O_2$ emission signals obtained in H_2O at 1270 nm for the 10pM (a) non-etched and (b) etched SiO_2@$Ag_{(c)}$@SiO_2-RB nanoparticles. Air-equilibrated sample signals

are shown in green; signals for the N_2 purged samples are shown in red; and equation S5 trace fit to the data shown in black with the corresponding fit residuals plot shown in grey.

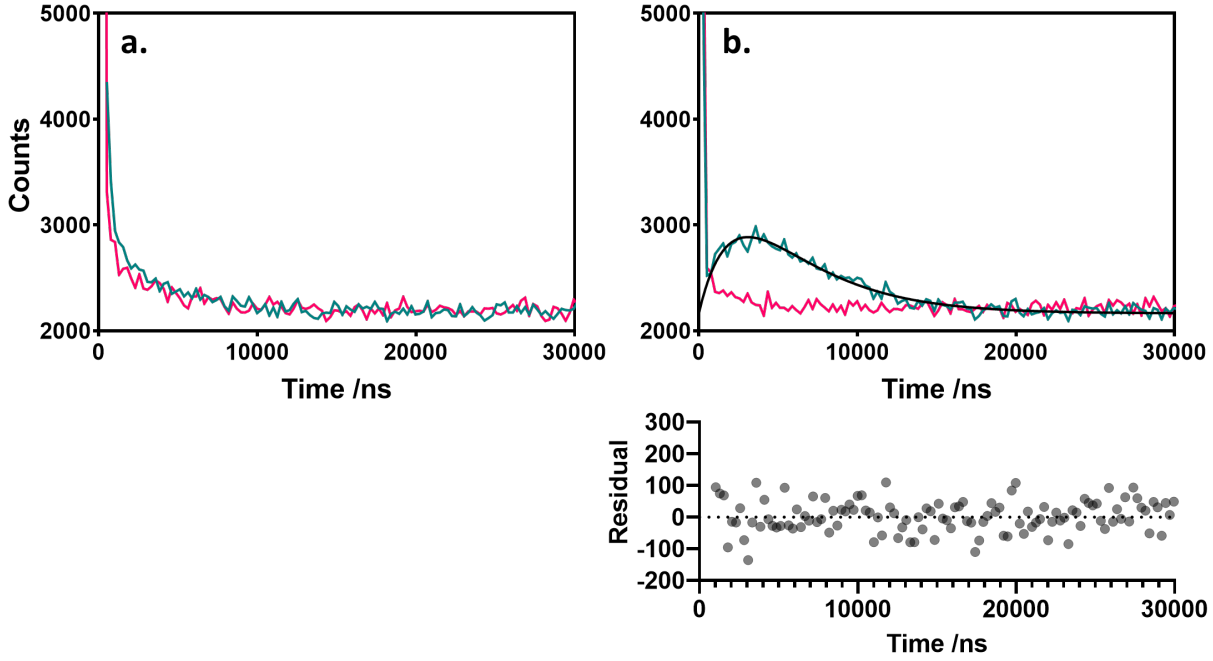

Figure S17: Time resolved direct detection of $^1O_2$ emission signals obtained in H_2O at 1270 nm for the 10pM (a) non-etched and (b) etched SiO_2@$Ag_{(p)}$@SiO_2-RB nanoparticles. Air-equilibrated sample signals are shown in green; signals for the N_2 purged samples are shown in red; and equation S5 trace fit to the data shown in black with the corresponding fit residuals plot shown in grey.

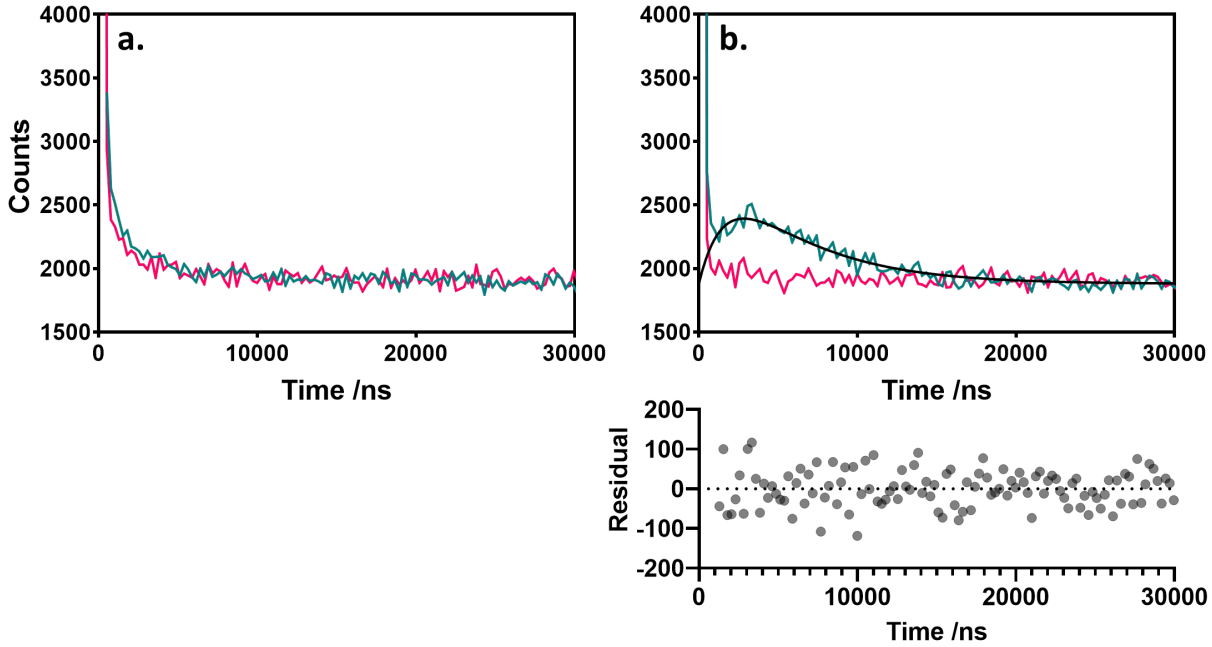

Figure S18: Time resolved direct detection of $^1O_2$ emission signals obtained in H_2O at 1270 nm for the 10pM (a) non-etched and (b) etched SiO_2@$Ag_{(i)}$@SiO_2-RB nanoparticles. Air-equilibrated sample signals are shown in green; signals for the N_2 purged samples are shown in red; and equation S5 trace fit to the data shown in black with the corresponding fit residuals plot shown in grey.

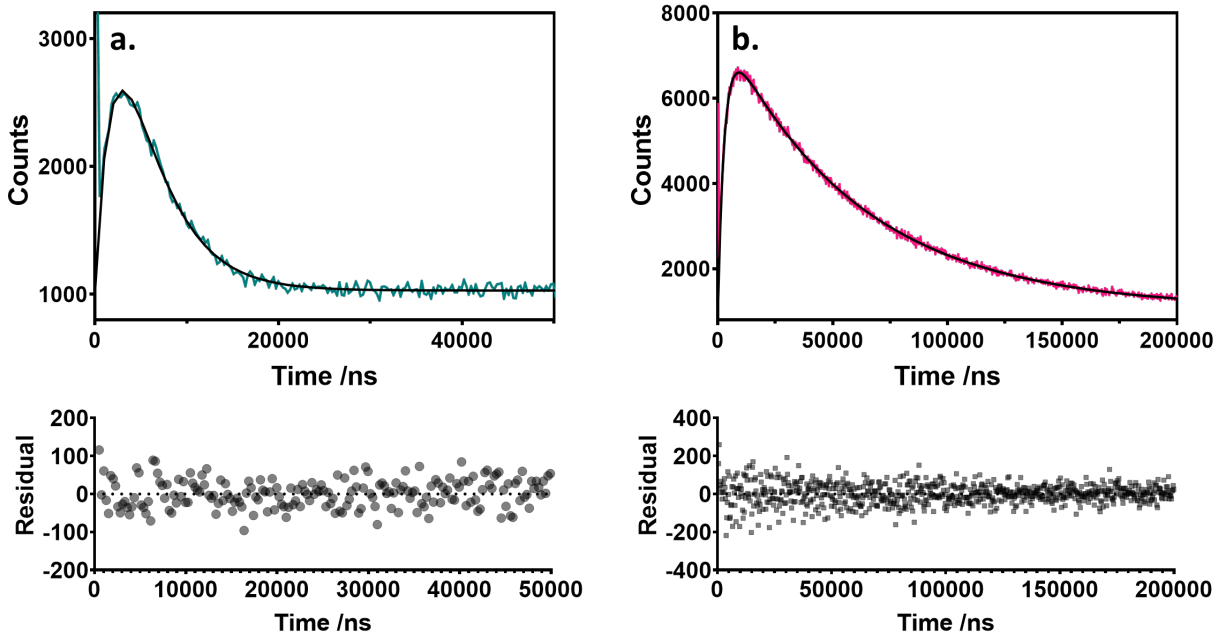

Figure S19: Time-resolved $^1O_2$ phosphorescence signals at 1270 nm (green and red) and the corresponding fittings (black) obtained on the sample of 2µM Rose Bengal photosensitizer in (a) H_2O; and in (b) 99% D_2O. Residuals obtained from the fits are shown in grey below each respective plot.

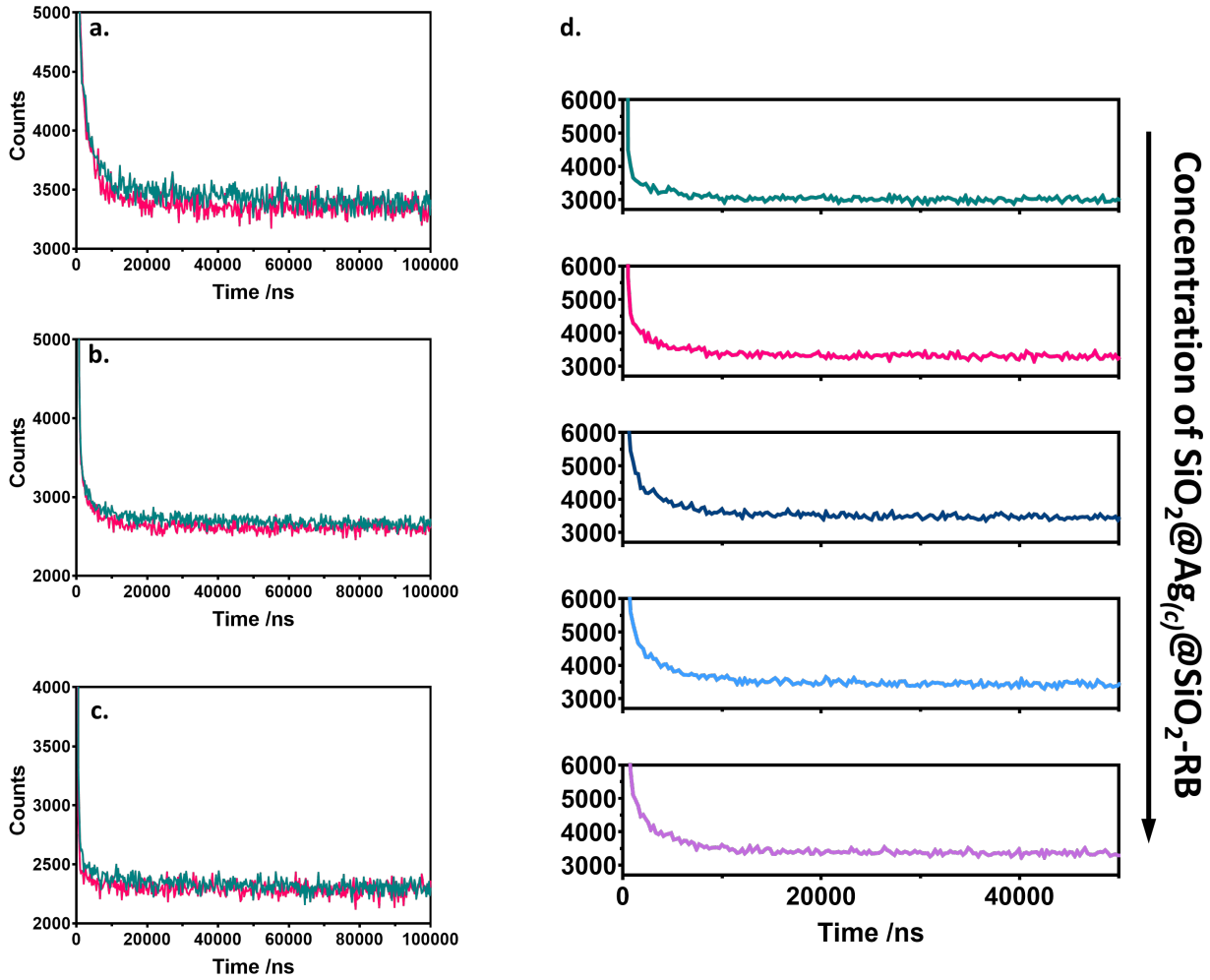

Figure S20: Time resolved direct detection of $^1O_2$ emission signals obtained in 99% D_2O at 1270 nm for the 10pM SiO_2@Ag@SiO_2-RB nanoparticles with (a) complete; (b) partial; and (c) incomplete silver shells. Air-equilibrated sample signals are shown in green; signals for the N_2 purged samples are shown in red. (d) Time resolved direct detection of $^1O_2$ emission signals obtained in 99% D_2O at 1270 nm for SiO_2@$Ag_{(c)}$@SiO_2-RB nanoparticles increasing in concentration from 2.5 pM to 12.5 pM (in 2.5 pM increments).

Table S1: Singlet oxygen phosphorescence decay curve fit parameters. †

	Etched SiO_2@$Ag_{(i)}$@SiO_2-RB in H_2O	***Etched SiO_2@$Ag_{(p)}$@SiO_2-RB in H_2O***	***Etched SiO_2@$Ag_{(c)}$@SiO_2-RB in H_2O***	***RB in H_2O***	***RB in D_2O***
S_0/counts	1090 ± 92	1495 ± 101	987 ± 63	3159 ± 75	6465 ± 6
τ_Δ/μs	4.1 ± 0.5	4.2 ± 0.4	4.9 ± 0.6	4.2 ± 0.1	59.1 ± 0.1
τ_T/μs	2.3 ± 0.3	2.3 ± 0.2	1.9 ± 0.2	2.2 ± 0.1	2.9 ± 0.02
Y_0/counts	1877 ± 1	2163 ± 1	2734 ± 1	1029 ± 1	1069 ± 2

† Errors are based on the standard deviation of fitting equation S5 to the experimental data

9. Steady-State Fluorescence Emission

Steady state fluorescence emission spectra were collected using PTI QuantaMaster 8000 fluorimeter. In all of the cases the slit widths were set to 2 nm on the excitation and on the emission sides. Emission scan was performed with the excitation wavelength set to 480 nm. All samples' emission was collected in H_2O. For scattering profiles, a solution of 120nm SiO_2 nanoparticles was used.

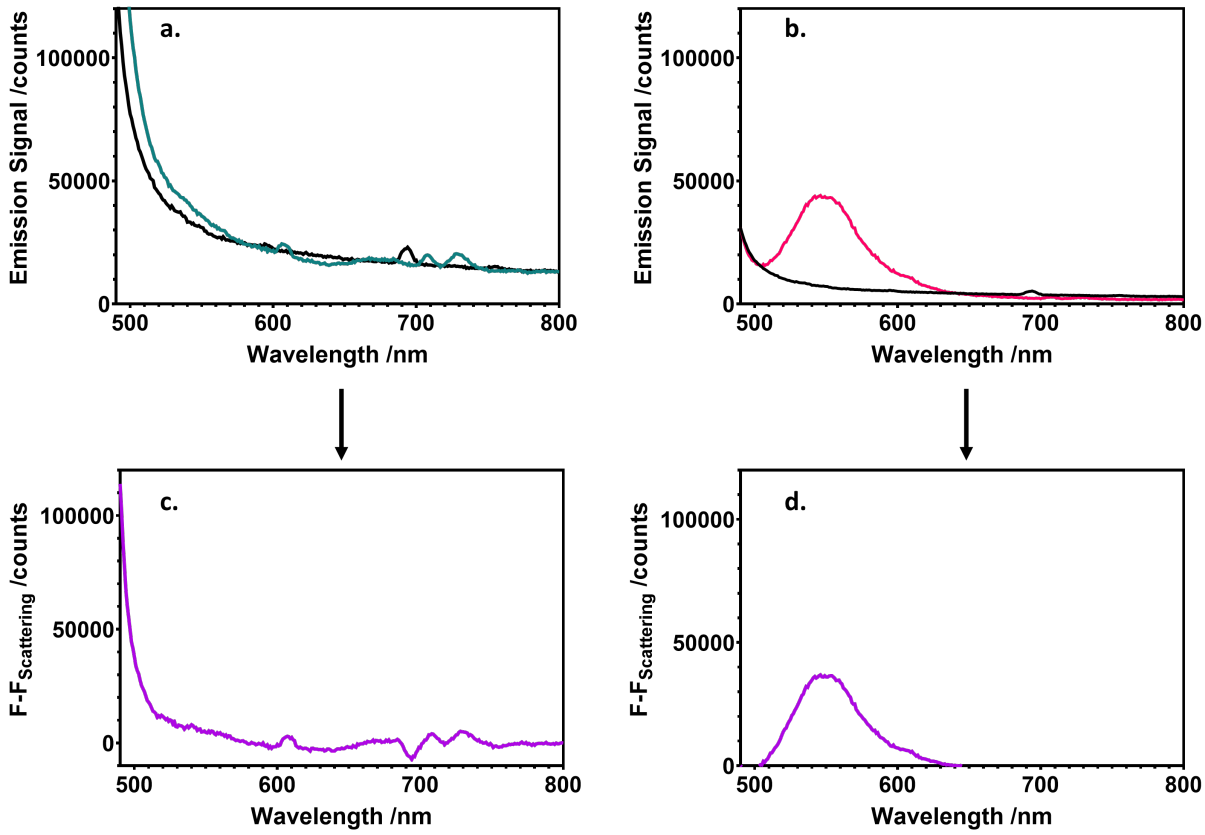

Figure S21: Fluorescence emission spectra of 10pM (a) non-etched SiO_2@$Ag_{(c)}$@SiO_2-RB nanoparticles (green) and their matched scattering profile (black); and (b) etched SiO_2@$Ag_{(c)}$@SiO_2-RB nanoparticles (red) and their matched scattering profile (black). Figures (c) and (d) are emission profiles of scattering-free non-etched and etched SiO_2@$Ag_{(c)}$@SiO_2-RB samples, respectively.

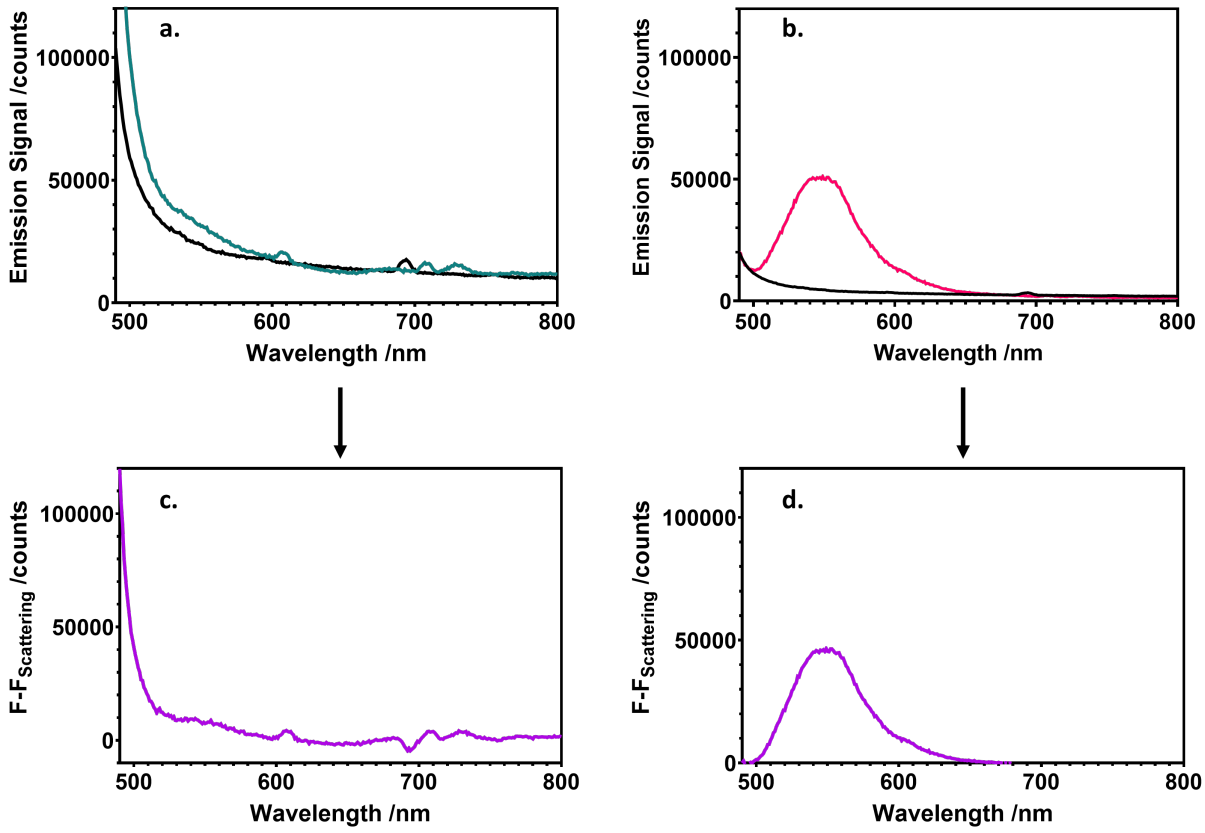

Figure S22: Fluorescence emission spectra of 10pM (a) non-etched SiO_2@$Ag_{(p)}$@SiO_2-RB nanoparticles (green) and their matched scattering profile (black); and (b) etched SiO_2@$Ag_{(p)}$@SiO_2-RB nanoparticles (red) and their matched scattering profile (black). Figures (c) and (d) are emission profiles of scattering-free non-etched and etched SiO_2@$Ag_{(p)}$@SiO_2-RB samples, respectively.

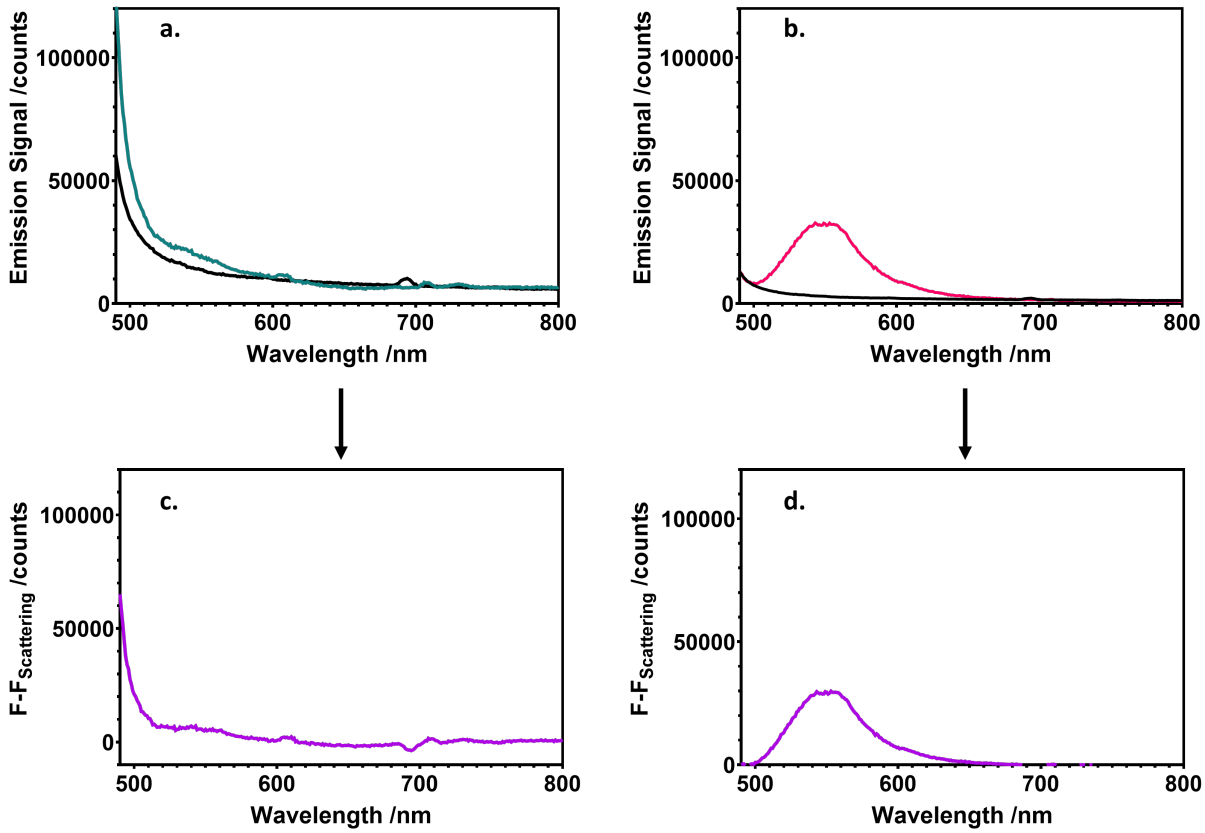

Figure S23: Fluorescence emission spectra of 10pM (a) non-etched SiO_2@$Ag_{(i)}$@SiO_2-RB nanoparticles (green) and their matched scattering profile (black); and (b) etched SiO_2@$Ag_{(i)}$@SiO_2-RB nanoparticles (red) and their matched scattering profile (black). Figures (c) and (d) are emission profiles of scattering-free non-etched and etched SiO_2@$Ag_{(i)}$@SiO_2-RB samples, respectively.

10. Indirect Detection of Singlet Oxygen

Irradiation of samples was performed using a CW halogen lamp (300 W, 80 V) mounted on a slide projector (Kodak) equipped with a 495 nm low-pass filter as to not directly irradiate the singlet oxygen detection probe (figure S24). Thorlabs digital optical energy and power meter console PM100D, equipped with S121C photodiode power sensor was used to measure light power received by the sample. Samples were set up to receive 10.0 ± 0.1 mW of light.

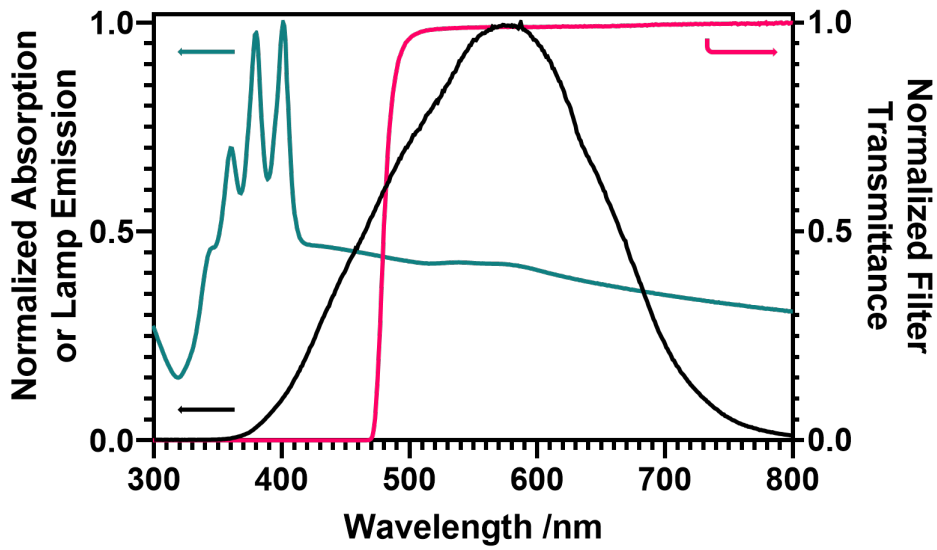

Figure S24: Spectral profile of the Kodak projector lamp used for sample's irradiation (black), and the UV-Vis transmittance of the 495 nm long-pass filter (red). Additionally shown is the normalized absorption spectrum of SiO_2@$Ag_{(p)}$@SiO_2-RB nanoparticle aqueous suspension with added ABDA probe (green). Arrows point each spectrum to the corresponding axis.

The following photochemical processes, with the corresponding rate constants, must be considered in a solution containing a $^1O_2$ sensor, ABDA, after excitation of a PS:

Light absorbance:	$^1PS + h\nu \rightarrow {}^1PS^*$	
Intersystem crossing:	$^1PS^* \rightarrow {}^3PS^*$	k_{ISC}
Energy transfer:	$^3O_2 + {}^3PS^* \rightarrow {}^1O_2 + {}^1PS$	k_{ET}
Singlet oxygen deactivation by the solvent:	$^1O_2 + H_2O \rightarrow {}^3O_2 + H_2O + \text{heat}$	$k_{\Delta, nr}$
Singlet oxygen light emission:	$^1O_2 \rightarrow {}^3O_2 + h\nu$	$k_{\Delta, r}$
Physical quenching by sensor:	$^1O_2 + ABDA \rightarrow {}^3O_2 + ABDA$	k_p
Chemical interaction with sensor:	$^1O_2 + ABDA \rightarrow ABDAO_2$	k_{ox}

We may first consider the case where the environment around the photosensitizer is homogeneous, i.e. a simple case of photosensitizer free in solution. Assuming that the direct reaction of PS in its ground state with the $^1O_2$ it produces is negligible. Under steady state approximation, i.e. no significant buildup of $^1O_2$ is expected, rate of the sensor disappearance can be written following equation S6, where the singlet oxygen production is a product of Φ_{PS}, representing the quantum yield of photosensitization, and I_{Abs} which is the intensity of light absorbed by the PS as defined by equation S7.

$$\frac{d[ABDA]}{dt} = -k_{ox}[ABDA][^1O_2] = -k_{ox}[ABDA]\frac{\Phi_{PS}I_{Abs}}{(k_{ox}+k_p)[ABDA]+k_{\Delta,nr}+k_{\Delta,r}} \qquad (S6)$$

$$I_{Abs} = \int_{\substack{absorption\\range}} I_{source}(\lambda) * T_{filter}(\lambda) * \left(1-10^{-A(\lambda)}\right) d\lambda \qquad (S7)$$

In our case the concentration of ABDA is small enough (10^{-4} M) to assume that the term *(k_{ox}+k_p)[ABDA]* is much smaller than the rate of singlet oxygen deactivation by the solvent *($k_{\Delta,nr}$ ≈ 3 × 10^5* M^{-1} s^{-1}*)*. Additionally, since singlet oxygen predominantly deactivates via the non-radiative pathway, over the radiative one, equation S6 can be altogether simplified to yield equation S8.

$$\frac{d[ABDA]}{dt} = -k_{ox}[ABDA]\frac{\Phi_{PS}I_{Abs}}{k_{\Delta,nr}} = -k_{PS} \times \Phi_{PS} \times I_{abs} \times [ABDA] \qquad (S8)$$

As stated above, equation S8 is derived for singlet oxygen which is produced from a photosensitizer present in a homogeneous environment. As we have shown in our previous studies,[5, 9] the case of photosensitizer bound to nanomaterials, i.e. heterogeneous environment, requires further modifications to said equation. In the case of the photosensitizer bound to the nanoparticles, $^1O_2$ can diffuse inside the nanomaterial's matrix where it will not encounter a probe molecule (in our case due to the tetra-anionic nature of ABDA and the highly negatively charged surface of silica coated nanoparticles), but rather will only be able to deactivate via its reaction with the solvent, or with the nanomaterial matrix itself. In our case, since the photosensitizer is bound to a silica outer shell, the following process must thus be accounted for:

Physical quenching by the nanomaterial: $^1O_2 + SiO_2 \rightarrow {}^3O_2 + SiO_2 + heat$ k_{nps}

This creates an asymmetry in the species deactivation in the context of its detection via a chemical probe. The overall rate of singlet oxygen deactivation (k_Δ^{total}) can now be represented following equation S9, where the values of *g* are each term's fractional contributions to k_Δ^{total} defined by equation S10.

$$k_\Delta^{total} = g^{out}\{(k_{ox}+k_p)[ABDA]+k_{\Delta,nr}\} + g^{in}(k_{\Delta,nr}+k_{nps}) + k_{\Delta,r} \qquad (S9)$$

$$g^{out} + g^{in} = 1 \qquad (S10)$$

Since the reaction between singlet oxygen and ABDA can only occur outside of the nanoparticles, equation S6 for a heterogeneous system in question can be re-written as equation S11.

$$\frac{d[ABDA]}{dt} = -g^{out}k_{ox}[ABDA][^1O_2] = -g^{out}k_{ox}[ABDA]\frac{\Phi_{PS}I_{Abs}}{k_\Delta^{total}} \qquad (S11)$$

Following a similar approach as was used to obtain equation S8, a simplified version of equation S11 can also be written as equation S12.

$$\frac{d[ABDA]}{dt} = = -g^{out} \times k'_{PS} \times \Phi_{PS} \times I_{abs} \times [ABDA] \qquad (S12)$$

Where, k'_{PS} is a combination of several constants defined by equation S13.

$$k'_{PS} = \frac{k_{ox}}{g^{out}k_{\Delta,nr} + g^{in}\left(k_{\Delta,nr} + k_{nps}\right) + k_{\Delta,r}} \qquad \text{(S13)}$$

Therefore, the integrated rate for the pseudo-first order reaction of ABDA and singlet oxygen produced from the SiO_2@Ag@SiO_2-RB nanoparticles can be written in the form of equation S14.

$$\ln[ABDA]_t = \ln[ABDA]_0 - (g^{out} \times k'_{PS} \times \Phi_{PS} \times I_{abs})t \qquad \text{(S14)}$$

By monitoring the ABDA degradation (figure S25), value of $(g^{out} \times k'_{PS} \times \Phi_{PS} \times I_{abs})$ term is determined experimentally as the slope of ABDA signal change processed in the pseudo-first order fashion (*m*). This is done for the non-etched (*ne*) and the etched (*e*) nanoparticle samples in order to quantify the effect of the silver shell on singlet oxygen production by calculating the singlet oxygen enhancement factor (EF_Δ), defined by equation S15.

$$EF_\Delta = \frac{(g^{out} \times k'_{PS} \times \Phi_{PS} \times I_{abs})_{\,ne}}{(g^{out} \times k'_{PS} \times \Phi_{PS} \times I_{abs})_{\,e}} = \frac{m_{ne}}{m_e} \qquad \text{(S15)}$$

Assuming singlet oxygen spends the same fraction of its lifetime in the bulk solvent environment regardless if the nanoparticles are etched or not, i.e. $g^{out}_{ne} = g^{out}_{e}$, the values of k'_{PS} will remain the same for the etched and non-etched nanoparticles (as per equations S10 and S13). Therefore, the enhancement factor is simplified to follow equation S16.

$$EF_\Delta = \frac{\Phi_{PS\,(ne)}}{\Phi_{PS\,(e)}} \times \frac{I_{abs\,(ne)}}{I_{abs\,(e)}} = \frac{m_{ne}}{m_e} \qquad \text{(S16)}$$

In it important to note that equation S16 can, and has been, previously derived just by treating the nanoparticle environment as homogeneous, i.e. directly from equation S8.[11, 12] However the thorough consideration of $^1O_2$ kinetics in the heterogeneous environment, presented above, is necessary to highlight the aforementioned justified assumptions undertaken in defining the EF_Δ parameter. Quantitative results of the indirect detection experiments for the non-etched and the etched nanoparticle samples are summarized in table S2.

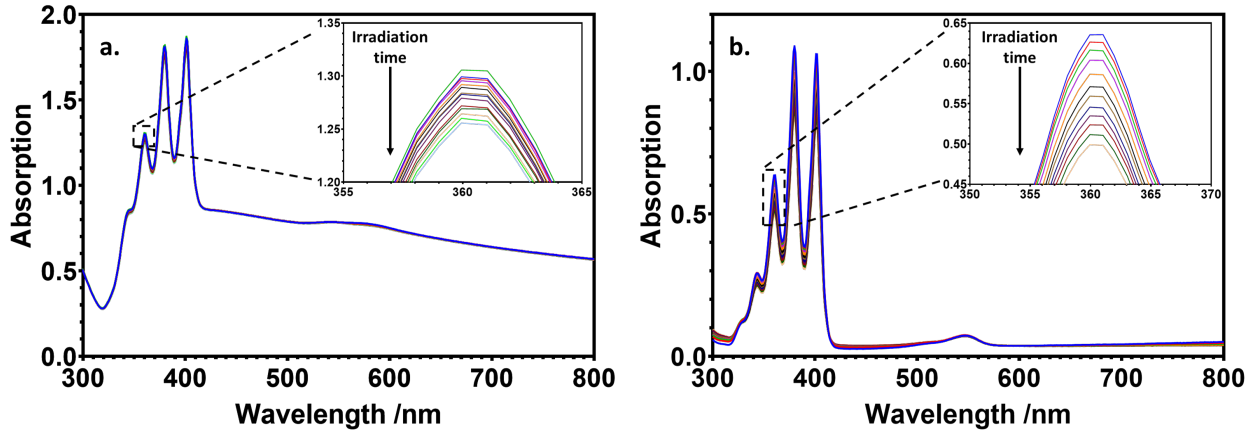

Figure S25: Sample UV-Vis data of singlet oxygen indirect detection experiments from (a) non-etched, and (b) etched SiO_2@$Ag_{(p)}$@SiO_2-RB nanoparticles in H_2O. Insets show the changes in ABDA absorption monitored throughout the indirect detection experiments.

Table S2: Results of the indirect detection of singlet oxygen from the non-etched and etched nanoparticle samples. †

Sample	*SiO_2 outer shell thickness /nm*	*m_{ne} /10^{-4} sec $^{-1}$*	*m_e /10^{-4} sec $^{-1}$*	*EF_Δ*
SiO_2@$Ag_{(i)}$@SiO_2-RB	12 ± 1	1.11 ± 0.04	3.47 ± 0.04	0.32 ± 0.02
SiO_2@$Ag_{(p)}$@SiO_2-RB	10 ± 1	1.17 ± 0.01	4.52 ± 0.07	0.259 ± 0.005
SiO_2@$Ag_{(c)}$@SiO_2-RB	12 ± 1	0.66 ± 0.01	3.41 ± 0.03 *	0.195 ± 0.003
SiO_2@$Ag_{(c)}$@SiO_2-RB	16 ± 2	0.58 ± 0.01		0.170 ± 0.003

† Errors are based on the standard deviation of fitting equation S13 to the processed experimental data.
* Indirect detection was performed on etched SiO_2@$Ag_{(c)}$@SiO_2-RB nanoparticles with 12 ± 1 nm outer SiO_2 shell to obtain the value of m_e for both SiO_2@$Ag_{(c)}$@SiO_2-RB with ~12 and ~16 nm outer SiO_2 shells.

11. Integrated Absorption Analysis

Considering that the linear combination of the transmission spectra of RB and the nanoparticle SiO_2@Ag@SiO_2 is similar the one of the SiO_2@Ag@SiO_2-RB, as supported by figure S26 below, the following integrated absorption analysis was carried out.

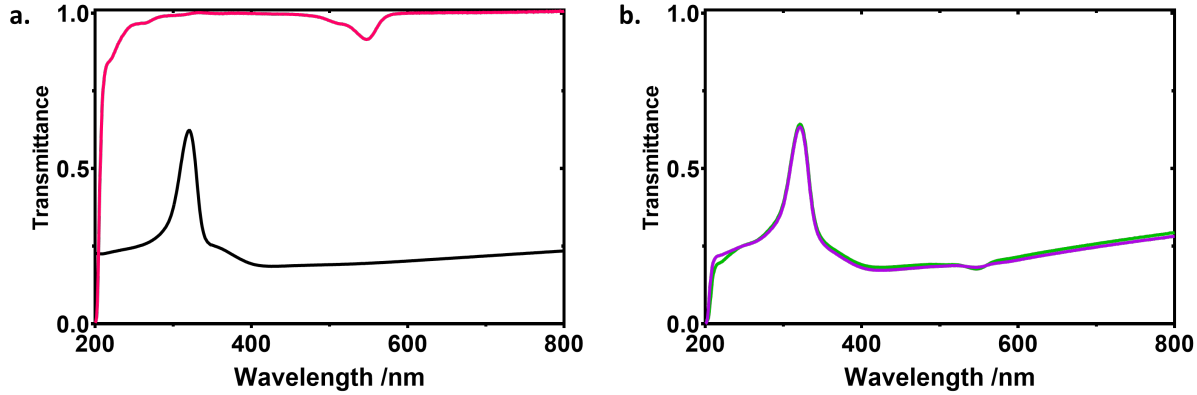

Figure S26: (a) Transmittance spectra of etched SiO_2@$Ag_{(p)}$@SiO_2-RB nanoparticles (red); and SiO_2@$Ag_{(p)}$@SiO_2 nanoparticles not modified with RB (black). (b) Combined transmittance of etched SiO_2@$Ag_{(p)}$@SiO_2-RB nanoparticles and SiO_2@$Ag_{(p)}$@SiO_2 nanoparticles not modified with RB, together representing a "computed" non-etched SiO_2@$Ag_{(p)}$@SiO_2-RB nanoparticles transmittance (green); and actual transmittance of non-etched SiO_2@$Ag_{(p)}$@SiO_2-RB nanoparticles (purple).

Integrated absorption of Rose Bengal ($I_{abs(RB)}$) under our experimental conditions was calculated following equation S17 and using the UV-Vis spectrum of the etched nanoparticles samples in order to most closely represent $I_{abs\ (e)}$.

$$I_{abs\ (e)} = I_{abs(RB)} = \int_{480\ nm}^{600\ nm} I_{source}(\lambda) * T_{filter}(\lambda) * \left(1 - 10^{-A(\lambda)}\right) d\lambda \qquad (S17)$$

In the case of calculating the $I_{abs\ (ne)}$ values, similarly to the etched samples, UV-Vis measurements of the etched nanoparticles were used for RB spectra. The individual extinction spectra of SiO_2@Ag@SiO_2 nanoparticles with incomplete, partial and complete silver shells were obtained at concentrations and optical densities most closely matching those of the indirect detection measurements; these spectra were converted to read transmission values ($T_{NPS}(\lambda)$) and used in equation S18 to obtain $I_{abs(RB+NPS)}$.

$$I_{abs\ (ne)} = I_{abs(RB+NPS)} = \int_{480\ nm}^{600\ nm} I_{source}(\lambda) * T_{NPS}(\lambda) * T_{filter}(\lambda) * \left(1 - 10^{-A(\lambda)}\right) d\lambda \qquad (S18)$$

Figures S27 – S29 present the data used in the integrated absorption calculations, with the results summarized in table S3.

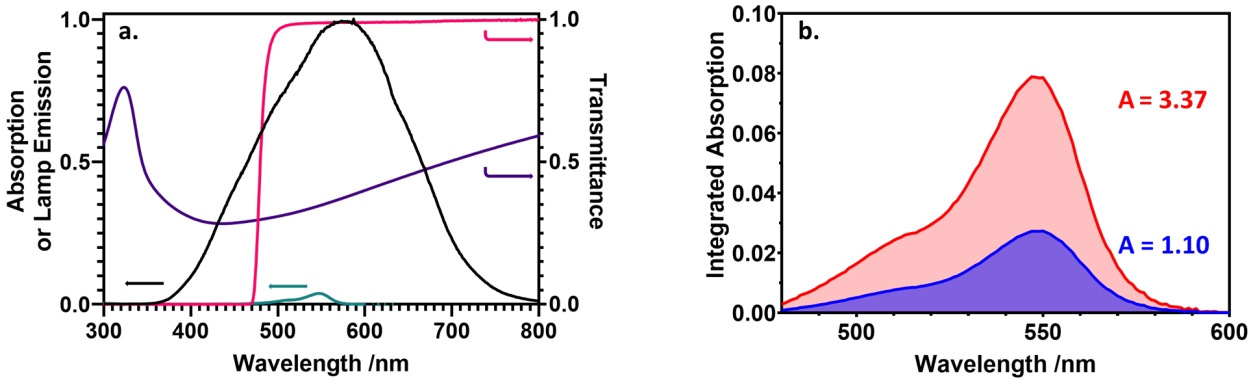

Figure S27: (a) Spectral profile of the Kodak projector lamp used for sample's irradiation (black); the UV-Vis transmittance of the 495 nm long-pass filter (red); the transmission spectrum of $SiO_2@Ag_{(i)}@SiO_2$ nanoparticles in aqueous suspension (purple), and the UV-Vis spectrum of RB from the fully etched $SiO_2@Ag_{(i)}@SiO_2$-RB nanoparticles (green). (b) Processed curves and their respective areas integrated following equations S17 (red) and S18 (blue). Arrows point each spectrum to the corresponding axis.

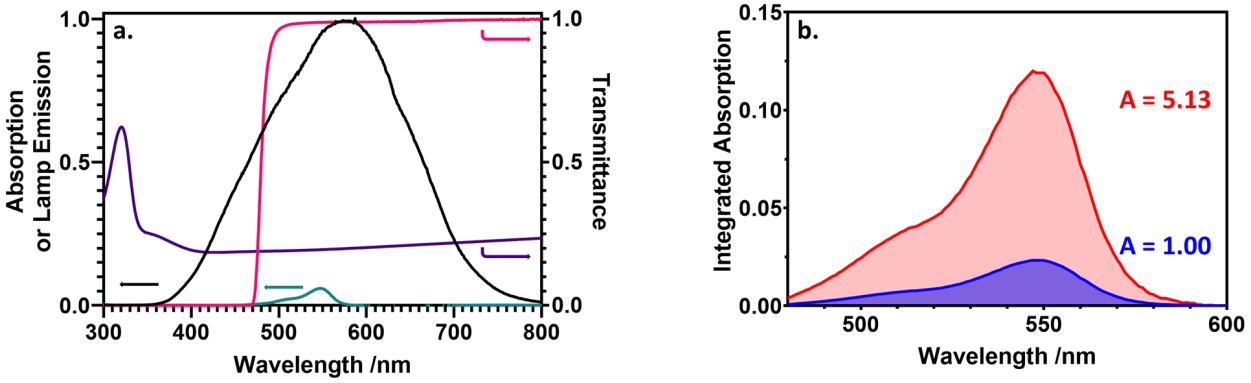

Figure S28: (a) Spectral profile of the Kodak projector lamp used for sample's irradiation (black); the UV-Vis transmittance of the 495 nm long-pass filter (red); the transmission spectrum of $SiO_2@Ag_{(p)}@SiO_2$ nanoparticles in aqueous suspension (purple), and the UV-Vis spectrum of RB from the fully etched $SiO_2@Ag_{(p)}@SiO_2$-RB nanoparticles (green). (b) Processed curves and their respective areas integrated following equations S17 (red) and S17 (blue). Arrows point each spectrum to the corresponding axis.

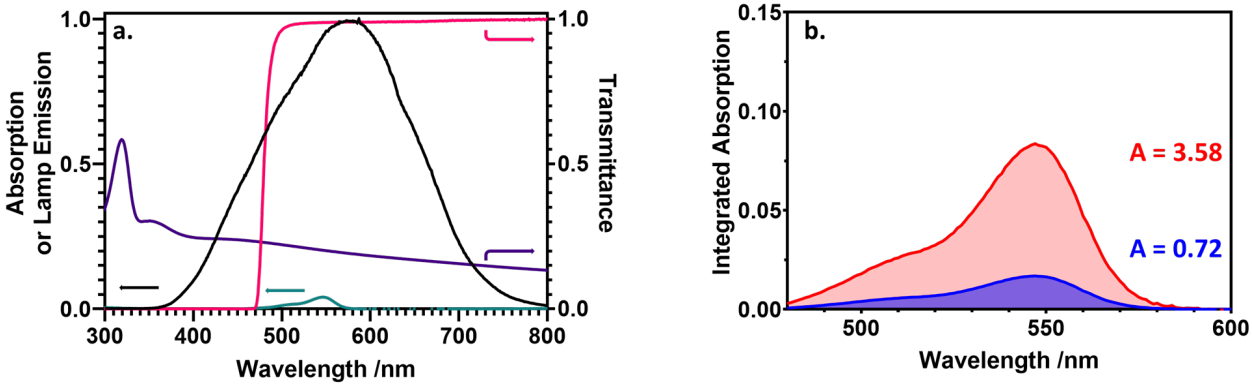

Figure S29: (a) Spectral profile of the Kodak projector lamp used for sample's irradiation (black); the UV-Vis transmittance of the 495 nm long-pass filter (red); the transmission spectrum of $SiO_2@Ag_{(c)}@SiO_2$ nanoparticles in aqueous suspension (purple), and the UV-Vis spectrum of RB from the fully etched $SiO_2@Ag_{(c)}@SiO_2$-RB nanoparticles (green). (b) Processed curves and their respective areas integrated following equations S17 (red) and S17 (blue). Arrows point each spectrum to the corresponding axis.

Table S3: Results of the integrated absorption calculations

Sample	$I_{Abs(RB+NPS)}$	$I_{Abs(RB)}$	$\frac{I_{abs\ (ne)}}{I_{abs\ (e)}}$
$SiO_2@Ag_{(i)}@SiO_2$-RB	1.10	3.37	0.327
$SiO_2@Ag_{(p)}@SiO_2$-RB	1.00	5.13	0.194
$SiO_2@Ag_{(c)}@SiO_2$-RB	0.72	3.58	0.201

References

1. Alberto, G.; Miletto, I.; Viscardi, G.; Caputo, G.; Latterini, L.; Coluccia, S.; Martra, G., Hybrid Cyanine−Silica Nanoparticles: Homogeneous Photoemission Behavior of Entrapped Fluorophores and Consequent High Brightness Enhancement. *The Journal of Physical Chemistry C* **2009,** *113* (50), 21048-21053.
2. Macia, N.; Kabanov, V.; Côté-Cyr, M.; Heyne, B., Roles of Near and Far Fields in Plasmon-Enhanced Singlet Oxygen Production. *The Journal of Physical Chemistry Letters* **2019,** *10* (13), 3654-3660.
3. Macia, N.; Kabanov, V.; Heyne, B., Rationalizing the Plasmonic Contributions to the Enhancement of Singlet Oxygen Production. *The Journal of Physical Chemistry C* **2020,** *124* (6), 3768-3777.
4. Nonell, S.; Braslavsky, S. E., [4] Time-resolved singlet oxygen detection. In *Methods in Enzymology*, Academic Press: 2000; Vol. 319, pp 37-49.
5. Kabanov, V.; Ghosh, S.; Lovell, J. F.; Heyne, B., Singlet oxygen partition between the outer-, inner- and membrane-phases of photo/chemotherapeutic liposomes. *Physical Chemistry Chemical Physics* **2019,** *21* (45), 25054-25064.
6. Hurst, J. R.; Schuster, G. B., Nonradiative Relaxation of Singlet Oxygen in Solution. *Journal of the American Chemical Society* **1983,** *105* (18), 5756-5760.

7. Schmidt, R.; Brauer, H. D., Radiation Deactivation of Singlet Oxygen (1Ag) by Solvent Molecules. *Journal of the American Chemical Society* **1987,** *109* (23), 6976-6981.
8. Zampini, G.; Planas, O.; Marmottini, F.; Gulias, O.; Agut, M.; Nonell, S.; Latterini, L., Morphology effects on singlet oxygen production and bacterial photoinactivation efficiency by different silica-protoporphyrin IX nanocomposites. *RSC Advances* **2017,** *7* (24), 14422-14429.
9. Kabanov, V.; Press, D. J.; Huynh, R. P. S.; Shimizu, G. K. H.; Heyne, B., Assessment of encapsulated dyes' distribution in silica nanoparticles and their ability to release useful singlet oxygen. *Chemical Communications* **2018,** *54* (49), 6320-6323.
10. Boso, G.; Ke, D.; Korzh, B.; Bouilloux, J.; Lange, N.; Zbinden, H., Time-resolved singlet-oxygen luminescence detection with an efficient and practical semiconductor single-photon detector. *Biomed. Opt. Express* **2016,** *7* (1), 211-224.
11. Macia, N.; Bresoli-Obach, R.; Nonell, S.; Heyne, B., Hybrid Silver Nanocubes for Improved Plasmon-Enhanced Singlet Oxygen Production and Inactivation of Bacteria. *Journal of the American Chemical Society* **2019,** *141* (1), 684-692.
12. Planas, O.; Macia, N.; Agut, M.; Nonell, S.; Heyne, B., Distance-Dependent Plasmon-Enhanced Singlet Oxygen Production and Emission for Bacterial Inactivation. *Journal of the American Chemical Society* **2016,** *138* (8), 2762-2768.